Molecular Pharmacology Fast Forward. Published on May 28, 2014 as doi:10.1124/mol.114.093310

MOL #93310

Molecular mechanisms of methoctramine binding and selectivity at muscarinic acetylcholine receptors

Jan Jakubík, Pavel Zimčík, Alena Randáková, Květoslava Fuksová, Esam E. El-Fakahany, Vladimír Doležal

Institute of Physiology (JJ, PZ, AR and VD) and Institute of Experimental Botany (KF), Academy of Sciences of the Czech Republic, 14220 Prague, Czech Republic, and Department of Experimental and Clinical Pharmacology, University of Minnesota College of Pharmacy, Minneapolis, MN 55455, USA (EEE).

Running Title: Mechanism of methoctramine binding

Correspondence to: Jan Jakubík

Inst. of Physiology AS CR, v.v.i.

Vídeňská 1083

142 20 Praha

Czech Republic

E-mail: jakubik@biomed.cas.cz

Phone: +420-2-4106-2620

Fax: +420-2-4106-2488

Pages: 31

Tables: 3

Figures: 11

References: 31

Abstract: 238 words

Introduction: 429 words

Discussion: 1495 words

Abbreviations: FRET, fluorescence resonance energy transfer; NMS, N-methylscopolamine; PCR, polymerase chain reaction

Abstract

Methoctramine (N,N'-bis[6-[[(2-methoxyphenyl)-methyl]hexyl]-1,8-octane diamine) is an M_2-selective competitive antagonist of muscarinic acetylcholine receptors and exhibits allosteric properties at high concentrations. To reveal the molecular mechanisms of methoctramine binding and selectivity we took advantage of reciprocal mutations of the M_2 and M_3 receptors in the second and the third extracellular loops that are involved in binding of allosteric ligands. To this end we performed measurements of kinetics of the radiolabeled antagonists N-methylscopolamine (NMS) in the presence of methoctramine and its precursors, fluorescence energy transfer between GFP-fused receptors and an Alexa-555 conjugated precursor of methoctramine, and simulation of molecular dynamics of methoctramine association with the receptor. We confirm hypothesis that methoctramine high-affinity binding to the M_2 receptors involves simultaneous interaction with both the orthosteric binding site and the allosteric binding site located between the second and third extracellular loops. Methoctramine can bind solely with low affinity to the allosteric binding site on the extracellular domain of NMS-occupied M_2 receptors by interacting primarily with glutamate 175 in the second extracellular loop. In this mode methoctramine physically prevents dissociation of NMS from the orthosteric binding site. Our results also demonstrate that lysine 523 in the third extracellular loop of the M_3 receptors forms a hydrogen bond with glutamate 219 of the second extracellular loop that hinders methoctramine binding to the allosteric site at this receptor subtype. Impaired interaction with the allosteric binding site manifests as low-affinity binding of methoctramine at the M_3 receptor.

Introduction

Five muscarinic receptor subtypes have been cloned (Bonner et al. 1987; Bonner 1989). They all belong to the family of G-protein-coupled receptors with seven transmembrane helices. The binding site of acetylcholine and competitive agonists and antagonists is located deep in a pocket formed by transmembrane helices (Wess 1996). All subtypes of muscarinic receptors share high homology in the transmembrane domains, making it difficult to discover competitive ligands that are selective for different receptor subtypes. However, a few such selective compounds have been identified. One example is methoctramine (N,N'-bis[6-[[(2-methoxyphenyl)-methyl]hexyl]-1,8-octane diamine) that binds to the M_2 subtype of muscarinic receptors with high affinity (Melchiorre et al., 1987) and to the M_3 subtype with low affinity (Caulfield, 1993). However, deviations from competitive behavior (slowdown of dissociation of orthosteric antagonists) at high concentrations of methoctramine were revealed soon after the discovery of its selectivity (Giraldo et al., 1988; Lee et al., 1989). Additional investigations have concluded that methoctramine interacts with muscarinic receptors both competitively and allosterically (Waelbroeck, 1994; Boselli and Grana, 1995), and the concept that methoctramine binds simultaneously to the orthosteric and allosteric receptor domains was proposed (Melchiorre et al., 1989). In the present work we provide experinmental support for this concept.

A large number of allosteric modulators selectively affect binding of the competitive ligands to M_2 receptors (Tuček and Proška, 1995). Several lines of evidence suggest that muscarinic allosteric ligands (e.g. gallamine and alcuronium) bind to the extracellular domain of muscarinic receptors (Leppik et al., 1994; Proška and Tuček, 1994; Jakubík and Tuček, 1994) and that amino acid residues in the second and the third extracellular loop are important for

this mode of binding (Leppik et al., 1994; Matsui et al., 1995; Gnagey et al., 1999; Krejčí and Tuček, 2001; Jakubík et al., 2005). In contrast, virtually nothing is known on nature of the selectivity of orthosteric muscarinic ligands.

In this study we investigated whether the extracellular domains of muscarinic receptors are also involved in putative allosteric properties of methoctramine binding and if they take part in high affinity of M_2 receptor for methoctramine. To achieve this aim we availed differences of methoctramine binding between the M_3 and M_2 receptor subtypes. We modified gene of the M_3 receptor in parts that encode the extracellular domains so that the resulting amino acid sequence resembles the one in the M_2 receptor. Using this approach we demonstrate that methoctramine selectivity for the M_2 receptor arises from its binding to glutamate residues in the second extracellular loop. A similar interaction at the M_3 receptor is prevented by interaction with K523 in the third extracellular loop.

Materials and Methods

Chemicals

N-[methyl -^{3}H]methylscopolamine ([^{3}H]NMS) was from NEN (Boston, MA), 4-difenylacetoxy-N-methylpiperidine (4-DAMP), 11-2[[2-[(diethylamino)methyl]-1-piperidinyl]acetyl]-5,11-dihydro-6H-pyrido[2,3-b][1,4] benzodiazepine-6-on (AF-DX 116) and N.N'-bis[6-[[(2-methoxyphenyl)-methyl]hexyl]-1,8-octane diamine (methoctramine) were from Tocris Cookson Ltd. (Avonmouth, UK), 4-[2-(1,6-dimethyl-piperidine-2-yl)-vinyl]-3-methyl-decahydro-naphto [2,3-c]furan-1-on (himbacine) and N-methylscopolamine were from Sigma (Prague, Czech republic). Succinimidyl ester of Alexa-555 carboxylic acid was from Life Technologies (Prague, Czech Republic). Synthesis of methoctramine precursors 6-aminohexyl)[(2-methoxyphenyl)methyl]amine and 8-amino-N-(6-{[(2-methoxyphenyl)methyl]amino}hexyl)octanamide and their conjugation with fluorescent label Alexa-555 is described in Supplemental Figure 1 and 2).

Mutagenesis and Expression

For the sake of brevity names of mutants consist of receptor subtype followed by a list of mutated amino acids in the third extracellular loop. Amino acids in either the M_2 or M_3 receptors were always mutated to the corresponding residue in the other receptor subtype (Supplemental Figure 3). For example, M_2 P means that proline 415 of the M_2 receptor was mutated to the corresponding serine in the M_3 sequence, and M_3 DSKFN means that five amino acids in the third extracellular loop of M_3 receptor were mutated to their corresponding residues in M_2 sequence.

The mammalian expression vector pcDNA3.1 (Invitrogen, Carlsbad, CA, USA) containing

the coding sequence of the human variants of M_2 and M_3 subtype of musarinic acetylcholine receptors were obtained from Missouri S&T cDNA Resource Center (Rolla, MO, USA). Construction of M_3 receptors with the substituted o2 loop and mutations (K523N, KFN and DSKFN) in the o3 loop were previously described in Krejčí and Tuček 2001. Additional mutants were generated using QuikChange II Site-Directed Mutagenesis Kit (Agilent Technologies Company, Santa Clara, CA, USA). To replace serine 519 with proline a plasmid containing wild-type M_3 receptor as template and 5'- TGA ACA CCT TTT GTG AC**C CC**T GCA TAC CCA AAA CCT TTT GG – 3' primer were used. To obtain DKFN mutant plasmid containing KFN mutant as template and 5'- GTG AAC ACC TTT TGT **GCC** AGC TGC ATA CCC AAT ACC-3' primer were used. To obtain SK mutant plasmid containing K523N mutant as template and 5'- TGA ACA CCT TTT GTG AC**C CC**T GCA TAC CCA ATA CCT TTT GG -3' primer were used. To obtain SKFN mutant plasmid containing KFN mutant and 5'- TGA ACA CCT TTT GTG AC**C CC**T GCA TAC CCA ATA CCG TTT GG-3' primer were used. To replace proline 415 of M_2 receptor with serine a plasmid containing wild-type M_2 receptor as template and 5'- AAC ACC TTT TGT GCA **TCT** TGC ATC CCC AAC ACT GTG-3' primer were used.

Chimeric proteins used in this study consist of three parts: chicken alpha 7 nicotinic signal peptide, emerald green fluorescent protein (GFP) and human muscarinic M_2 (hM_2) or M_3 (hM_3) receptor. DNA sequence of chicken alpha 7 nicotinic signal peptide (31 amino acids long peptide with extracellular protease cleavage site included, Ilien et al. 2003) was fused directly to stop-codon free GFP (Invitrogen) at its 5' end to assure extracellular localisation of fluorescent protein. cDNA for hM_2 receptor (cloned into pcDNA3.1+ vector) were mutated (QuikChange II Site-Directed Mutagenesis Kit) to obtain AgeI restriction site at 5' cDNA end. EcoRI and AgeI (New England BioLabs, Ipswitch, MA, USA) double digestion opened the

vector and created two cohesive ends for ligation. T4 ligation (New England BioLabs) reaction included opened hM_2 receptor vector, signal peptide-GFP complex and short linker. hM_2 cDNA was substituted with hM_3 cDNA to obtain GFP tagged hM_3 chimeric protein. All constructs were sequenced before use. Chimeric protein expression in eukaryotic cell lines were verified under fluorescent microscope and via ^{3}H-NMS binding (see bellow). All mutated DNAs were sequenced with the dideoxy method by Dr. J. Felsberg (Academy of Sciences, Institute of microbiology, Prague, Czech Republic).

COS-7 cells were transfected with the use of the DEAE-dextran method. They were grown in 10-cm Petri dishes in Iscove's modified Dulbecco's medium (Sigma) with 10% fetal calf serum. On day one 2×10^6 cells were seeded per dish. On day three after washing with phosphate-buffered saline, the transfection mix (2 µg of plasmid DNA and 0.27 mg of DEAE-dextran in 1 ml of phosphate-buffered saline) was applied for 2 h. Serum free Iscove's modified Dulbecco's medium with chloroquine (80 µM in 7 ml of medium) was then added for an additional 3 h. Transfection medium was then removed and fresh medium supplemented with 10 % fetal calf serum was applied. Cells were harvested 72 h after transfection.

Radioligand Binding Experiments

Radioligand binding experiments were performed on membranes of COS-7 cells. Membranes were obtained by dilution of freshly harvested COS-7 cells in a medium composed of 136 mM NaCl, 5 mM KCl, 1 mM $MgCl_2$, 10 mM EDTA and 10 mM Na-HEPES (pH=7.4) to a final concentration of 10^7 cells per ml. Cell suspension was homogenized using Ultra-Turrax homogenizer by two 30 second strokes. Homogenate was centrifuged 5 min at 1,000 x g. Resulting supernatant was centrifuged for 30 min at 30,000 x g and supernatant was

discarded. Pellet was resuspended in 10 times the original volume (before centrifugation), left at 4 °C for 30 min and then the latter centrifugation step was repeated. Membranes were kept frozen at -20 °C for a maximum of one month. Binding experiments to membranes from 1 to 2 million cells per tube were done as described earlier (Jakubík et al., 1995). The medium used for incubation was the same as described above without EDTA and incubation volume was 0.8 ml. Incubations performed at 25 °C were terminated by filtration through Whatman GF/C glass fiber filters in a Brandel filtration apparatus (Sensat, Herts, UK). Nonspecific binding was determined in the presence of 1 μM NMS.

The affinity of wild-type and mutated muscarinic receptors for [^{3}H]NMS was measured in saturation binding experiments (1 h incubation with [^{3}H]NMS at concentrations ranging from 32 pM to 1 nM), and expressed as $K_{d(NMS)}$ (equilibrium dissociation constant for the binding of [^{3}H]NMS). The inhibition constants K_i of receptors for methoctramine, 4-DAMP, AF-DX 116 and himbacine were determined in competition experiments in which membranes were incubated in the presence of a fixed 200 pM concentration of [^{3}H]NMS and increasing concentrations of the competitor. The incubation lasted 5 h to achieve full equilibrium. In dissociation experiments, membranes were preincubated for 1 h with 750 pM [^{3}H]NMS. Dissociation was induced by adding 50 μl of NMS to a final concentration of 1 μM. NMS was added either alone or in mixture with methoctramine or methoctramine precursors at final concentrations ranging from 10 pM to 1 mM.

Fluorescence resonance energy transfer

Fluorescence resonance energy transfer (FRET) between GFP-M_2 or GFP-M_3 receptors and conjugate of long methoctramine precursor (LMP) and Alexa-555 (Alexa-555-LMP) was measured in 96-well plates using Perkin Elmer Victor X4 plate reader. Following set of filters

from Knight Optical (Harrietsham, UK) was used: excitation 470/10 nm, GFP emission 532/10 nm, Alexa-555 emission 590/10 nm. Acquisition time was 0.1 s. Membranes prepared from COS-7 cells transiently transfected with GFP-M_2 or GFP-M_3 genes (about 50 µg of protein per well) were used. Association was initiated by addition of Alexa-555-LMP to final concentrations ranging from 30 nM to 1 µM. Dissociation was started by addition of methoctramine to a final concentration of 1 mM. Final sample volume was 0.2 ml. Besides samples containing both fluorescent probes, wells with only GFP labeled receptors and Alexa-555-LMP (with added comparable amount of non-transfected COS-7 membranes) were measured to check for fluorescence bleaching. Up to 15 % of bleaching was observed for GFP during 6-hour experiment. No bleaching was observed for Alexa-555-LMP.

Data treatment

Data were processed and analyzed with open source software OpenOffice 3.4 (OpenOffice Foundation, www.openoffice.org) and Grace 5.1.12 (Grace Development Team, plasma-gate.weizmann.ac.il/Grace) on Scientific Linux (www.scientificlinux.org).

The equations for nonlinear regression analysis were as follows:

For saturation binding experiments:

After subtraction of nonspecific binding Eq. 1 was fitted to the data.

(Eq. 1) $$Y = B_{MAX} * X / (K_D + X)$$

where Y is [^{3}H]NMS binding at concentration X of free [^{3}H]NMS, K_D is the equilibrium dissociation constant, and B_{MAX} is the number of binding sites.

For competition experiments:

After subtraction of nonspecific binding and normalization (to express the binding of

[^{3}H]NMS in the presence of competitor (methoctramine, 4-DAMP, AF DX-116 or himbacine) as per cent of the binding in the absence of competitor) Equation 2 was fitted to the data.

(Eq. 2) $Y = 100 - 100 / (1+10^{(X - \log IC50)})$

where Y is [^{3}H]NMS binding at logarithm of concentration of competitor X, and IC_{50} is the concentration of competitor that results in 50 % of maximal inhibition. Inhibition constant K_i was calculated from IC_{50} value according Cheng and Prussof (1973) :

(Eq. 3) $K_i = IC_{50} / (1 + [NMS] / K_D)$

where [NMS] is actual concentration of [^{3}H]NMS used in experiment and K_D is equilibrium dissociation constant of [^{3}H]NMS.

Dissociation experiments:

After subtraction of nonspecific binding Eq. 4 was fitted to the data.

(Eq. 4) $Y = 100 * e^{(-Koff(obs) * X)}$

where Y is [^{3}H]NMS binding at time X, and $k_{off(obs)}$ is the observed dissociation rate constant. Apparent equilibrium dissociation constant K_D for methoctramine based on dissociation experiments was obtained according Lazareno and Birdsall (1995):

Eq. 5 $Y = k_0 * K_D / (X + K_D)$

where Y is observed rate of dissociation $k_{off(obs)}$ at concentration X of allosteric ligand (methoctramine or SMP) and k_0 is observed dissociation rate in the absence of allosteric ligand.

The error distributions for individual constants were verified according Christopoulos 1998. IC_{50} (Eq. 2), and consequently K_i (Eq. 3), and K_D (Eq. 5) have log-normal error distribution. Error distributions for NMS K_D (Eq. 1) and $k_{off(obs)}$ (Eq. 4) conform to normal Gaussian

distribution.

Parameters of binding kinetics from FRET measurements were obtained by fitting tandem two-site model (Jakubík et al., 2000) to the pooled data with subtracted background values using program COPASI (Hoops et al., 2006). Initial parameter estimates and background values were obtained by fitting two exponential growth and two exponential decay function, respectively, to the individual data sets using program Grace.

Molecular modeling

Preparation of structures and systems

Structure of methoctramine (CID 4108) was downloaded from PubChem database (pubchem.ncbi.nlm.nih.gov) and processed with Shrödingers' LigPrep. Crystal structures of M_2 (Haga et al., 2012) (PDB code 3UON) and M_3 (Kruse et al., 2012) (PDB code 4DAJ) receptors were downloaded from RCSB Protein Data Bank (www.rcsb.org), and pre-processed with Schrödingers' Protein Preparation Wizard to remove non-receptor parts, fill missing side chains and energy minimize structures in OPLSA 2005 force field. System consisting of receptor, DPPC (1,2-dipalmitoylphosphatidylcholine) membrane, water and 0.15 M NaCl with or without methoctramine randomly placed close to receptor extracellular domain was built with Desmond System Builder.

Simulation of molecular dynamics

Molecular dynamics of full membrane systems was simulated using Desmond (Bowers et al., 2006). First, systems were relaxed to 300 K using standard Desmond protocol for membrane systems and subsequently 120 ns of free (without restrains) molecular dynamics (MD) (ensemble class NVE, Coulombic short range method - cutoff with radius 9 Å, long range method – smooth particle mesh Evald) was simulated using Desmond-GPU.

Six systems with methoctramine were built and used for simulation of methoctramine

association. After system relaxation prior to free MD simulation 25 ps of steered MD was run during which acceleration of 500 $pm*ps^{-2}$ towards center of the orthosteric binding site (defined by D103 and N404) was applied to one of anisole groups of methoctramine. Steered MD and free MD were repeated until distance between centers of anisole group and the orthosteric binding site reached 5 Å. Then 500 ns of free MD was simulated.

Results

Equilibrium experiments - methoctramine

In preliminary experiments we measured the effects of replacement of the entire o2 or o3 loop of the M_3 receptor with the corresponding M_2 sequence on the binding of muscarinic the M_2 selective ligands AF-DX 116, himbacine and methoctramine (Fig. 1) and the M_3 selective ligand 4-DAMP. Replacement of the o2 loop of the M_3 receptor with that of the M_2 receptor did not change the affinity of the tested ligands except for 4-DAMP where affinity of the hybrid receptor fell far below the value of the M_2 wild type receptor (Table 1). Replacement of the o3 loop of the M_3 receptor with that of the M_2 receptor did not change the affinity of 4-DAMP, AF-DX 116 or for himbacine but increased the affinity of methoctramine to a value close to the one at the M_2 receptor.

In subsequent experiments we measured binding of methoctramine to the seven mutant receptors having mutations in the o3 loop. Mutation of serine 519 (M_3 numbering) to corresponding proline (M_3S) only slightly increased the affinity of methoctramine. Mutation of lysine 523 (M_3 numbering) to corresponding asparagine (M_3K) increased the affinity of methoctramine more than 6 times. Combination of M_3K mutation with the mutation of phenylalanine 525 to valine, asparagine 527 to threonine and aspartate 518 to alanine, i.e. M_3KFN and M_3DKFN, respectively, did not further change the affinity of methoctramine. Double-mutation M_3SK increased the affinity of methoctramine to a value close to the one at the wild type M_2receptor. Combination of the double-mutation M_3SK with mutation of F525, N527 and D518, i.e. M_3 SKFN and M_3 DSKFN, did not further change the affinity of methoctramine (Table 2). Taken together, only the M_3S and M_3K mutations increased affinity of methoctramine. Mutation M_3K contributed most to affinity increase. In accordance with

these observations, mutation of proline 415 (M_2 numbering) in o3 loop of M_2 receptor to serine, i.e. M_2P, brought about a 10-fold decrease in affinity of methoctramine (Table 2).

Kinetic Experiments - methoctramine

Kinetic binding experiments were performed to ascertain putative allosteric properties of methoctramine. Membranes were first preincubated with [^{3}H]NMS for 1 hour then dissociation was started by the addition of unlabeled NMS to a final concentration of 1 μM, either alone or in mixture with various concentrations of methoctramine. In the absence of methoctramine dissociation of [^{3}H]NMS from the M_2 receptors is about 6 times faster than that from M_3 receptors (Fig. 3, Table 3). In the presence of 100 μM methoctramine the dissociation from the M_2 receptor was slowed down > 50 fold (Fig. 3 top, Table 3). In contrast, the observed dissociation rate of [^{3}H]NMS from the M_3 receptor did not significantly differ in the presence of 100 μM methoctramine (Fig. 3 bottom, Table 3).

Interestingly, all tested mutations in the o3 loop of M_3 receptor except M_3S accelerated [^{3}H]NMS dissociation in the absence of methoctramine (second column of Table 3). The rate of [^{3}H]NMS dissociation at M_3KFN, M_3SKFN and M_3DSKFN receptors was the same as that at the wild type M_2 receptor. Moreover, there was a significant difference in [^{3}H]NMS dissociation rate at M_3KFN and M_3DKFN vs. M_3K. Also [^{3}H]NMS dissociation from M_3 SKFN and M_3 DSKFN mutants was significantly faster than from M_3SK but there was no difference in dissociation from M_3KFN, M_3SKFN and M_3DSKFN as well as from M_3 K and M_3 SK. Taken together, although all mutations except M_3S accelerate [^{3}H]NMS dissociation, mutation of F525 to valine and N527 to threonine have the most profound effect on dissociation of [^{3}H]NMS.

[^{3}H]NMS dissociation in the presence of 100 μM methoctramine was slower at all mutants

(except for M_3S) than at the M_3 wild type. In fact, the rate of radioligand dissociation at M_3DKFN, M_3SK, M_3SKFN and M_3DSKFN mutants was the same as at the M_2wt (third column of Table 3). In other words, mutation of only a single residue, K523 to asparagine, elicited allosteric interaction between methoctramine and [^{3}H]NMS on M_3 receptor inferred from accelerating the speed of dissociation. In accordance with these observations, mutation of P415 in the o3 loop of M_2 receptor to serine, i.e. M_2 P, did not change [^{3}H]NMS dissociation significantly, either in the absence or in the presence of methoctramine (Table 3). Only mutations of K523, F525 and N527 (i.e. M_3KFN, M_3DKFN, M_3SKFN, and M_3DSKFN) significantly altered the ratio of $K_{off(obs)}$ in the absence of methoctramine to $K_{off(obs)}$ in the presence of 100 μM methoctramine (fourth column of Table 3). Again, this parameter was the same for the M_3SKFN, M_3DSKFN and the M_2wt receptor.

In the next set of experiments, we measured the effects of various concentrations of methoctramine on [^{3}H]NMS dissociation on wild type receptors and all mutants. The observed dissociation rate constants ($K_{off(obs)}$) were calculated according to Eq. 4. Calculated $K_{off(obs)}$ were plotted as a function of methoctramine concentration (Fig. 4). Values of apparent equilibrium dissociation constants (K_D) for methoctramine binding to [^{3}H]NMS-occupied receptors were obtained by fitting Eq. 5 to the data in Fig. 4 (top) and are shown in Table 3. Except for the M_3S mutant the calculated K_Ds are close to K_D of M_2wt. In other words, mutation of K523 (M_3K) is crucial for allosteric properties of methoctramine binding.

To get deeper insight into the mechanisms underlying methoctramine slowing down of [^{3}H]NMS dissociation we measured [^{3}H]NMS dissociation from M_2 receptors in the presence of concentrations of methoctramine that saturate its binding to [^{3}H]NMS-occupied receptors (Fig. 4 bottom). Dependence of $K_{off(obs)}$ on the concentration of methoctramine fits well Eq. 5 (pK_D = 5.2 ± 0.2 (mean ± S.E.M., n=3)). A good fit to Eq. 5 even at high methoctramine

concentrations means that dissociation limits to 0, i.e. methoctramine prevents radioligand dissociation completely.

Equilibrium experiments – methoctramine precursors

To get insight into substuctures of methoctramine responsible for interaction with the receptor we synthesized a short and a long methoctramine precursors, namely 6-aminohexyl)[(2-methoxyphenyl)methyl]amine (SMP) and 8-amino-N-(6-{[(2-methoxyphenyl)methyl]amino}hexyl)octanamide (LMP) (Fig. 1). Binding of these precursors was measured at M_2 and M_3 wild-type receptors and M_3 S, M_3 K,M_3 SK and M_3 DSKFN mutants. Affinity of SMP was lower than the affinity of methoctramine at both M_2 and M_3 wild-type receptors while affinity of LMP was lower than affinity of methoctramine only at M_2 receptor (Fig. 5). Moreover at M_2 receptor SMP affinity was lower by 100 fold while LMP affinity was lower only 3 times than affinity of methoctramine (Table 2). Both single mutations in the o3 loop of the M_3 receptor, S519P (M_3 S) and K523N (M_3 K), increased the affinity of both precursors. Similar to methoctramine the increase in affinity was greater at M_3 K than at M_3 S. Mutants M_3 SK and M_3 DSKFN displayed the same affinity for both precursors as at M_2 wt.

Kinetic experiments – SMP

To test the allosteric properties of SMP we tested its effects on [^{3}H-NMS] dissociation as described above for methoctramine. In the presence of 100 μM SMP radioligand dissociation from the M_2 wt receptor was slowed down by more than 30-fold (Fig. 6, Table 3). In contrast, similar to methoctramine, effects of 100 μM SMP on [^{3}H]NMS dissociation from M_3 wt receptor was marginal (Fig. 6, Table 3). Similar to methoctramine, [^{3}H]NMS dissociation in the presence of 100 μM SMP was slower at all mutants than at the M_3 wt receptor, with the

exception of M_3S. At M_3SK and M_3DSKFN mutants [^{3}H]NMS dissociation was as slow as at the M_2 wt receptor. Values of apparent equilibrium dissociation constants (K_D) for SMP binding to [^{3}H]NMS-occupied receptors were obtained by fitting Eq. 5 to the data in Fig. 6 (top) and are shown in Table 3. Except for the M_3S mutant the calculated K_Ds are close to the K_D at the M_2 wt receptor. Importantly, K_Ds of SMP were the same as those of methoctramine. As in the case of methoctramine, dependence of $K_{off(obs)}$ of dissociation from the M_2 wt receptor at concentrations of SMP that saturate binding to [^{3}H]NMS-occupied receptors (Fig. 6 bottom) fits well Eq. 5 ($pK_D = 5.5 \pm 0.2$ (mean ± S.E.M., n=3)).

Kinetics experiments – FRET

For fluorescence resonance energy transfer (FRET) measurements we constructed emerald green fluorescent protein (GFP) attached to N-terminus of either M_2 wt or M_3 wt receptors as donors. As an acceptor LMP was conjugated with Alexa-555 (Supplemental Methods). Attachment of GFP to the N-termini of the receptors did not change their binding properties as assessed in [^{3}H]NMS saturation and competition experiments (Supplemental Table 1). The affinity of LMP-Alexa-555 in competition experiments with [^{3}H]NMS at M_2 wt and M_3 wt receptors was the same as that of LMP (Supplemental Table 1). Measurements of FRET allowed direct assessment of binding kinetics of LMP-Alexa-555 (Fig. 7 and 8). LMP-Alexa-555 was added to membranes from COS-7 cells transiently expressing GFP-M_2 receptors (Fig. 7) at final concentration of 30 nM (top), 100 nM (middle) and 300 nM (bottom) and FRET signal was followed for 4 hours (black). Dissociation was initiated by the addition of methoctramine at a final concentration of 1 mM either after 5 (red), 60 (green) or 120 min of association. Association was bi-phasic with a very rapid initial phase followed by a phase with an observed association rate around 0.02 min^{-1} (analytical data are in Supplemental Table 2). Nonspecific signal was very strong, being about two thirds of total

signal under equilibrium even at the lowest concentration. With increasing concentrations specific signal increased as well as proportion of fast association that rose from 15 % at 30 nM to 53 % at 300 nM. The observed association rate of the slower phase remained the same. Dissociation of LMP-Alexa-555 from M_2 receptors was also bi-phasic. The rate of the fast dissociation phase could not be determined as it was below assay resolution. The rate of slow dissociation was around 0.007 min^{-1}. The proportion of slow dissociation increased both with concentration of LMP and the length of association. The rate of slow dissociation was independent of both the duration of association and concentration used. Fitting a receptor-antagonist complex isomerization model (Järv et al., 1979) to the kinetic data in Fig. 7 using program COPASI provided the following results: k_{+1} = 2 x 10^8 $M^{-1}.min^{-1}$; k_{-1} = 100 min^{-1}; k_{+2} = 0.07 min^{-1}; k_{-2} = 0.008 min^{-1}.

Higher concentrations of LMP-Alexa-555 were used in FRET measurements at GFP-M_3 receptors because of the lower affinity of methoctramine and its precursors at the wild type M_3 receptor (Fig. 8). Even still higher concentrations of LMP-Alexa-555 would be required to get comparable occupancy at the M_3 receptors. However, at 3 µM concentration of LMP-Alexa-555 the background signal was already too strong and background noise obscured a specific signal. Due to slower kinetics of LMP-Alexa-555 at M_3 than M_2 receptors dissociation was initiated after 60 min (green), 2 hours (blue) and 4 hours (yellow) of association. Association was biphasic with a very rapid initial phase followed by a phase with observed association rate around 0.01 min^{-1} (analytical data are in Supplemental Table 3). Dissociation of LMP-Alexa-555 from M_3 receptors was also bi-phasic. The rate of the fast dissociation cannot be determined as it is below assay resolution. The rate of slow dissociation was around 0.004 min^{-1}. Fitting a receptor-antagonist complex isomerization model (Järv et al., 1979) to the kinetic data in Fig. 8 using program COPASI gave the

following results: k_{+1} = 2 x 10^8 $M^{-1}.min^{-1}$; k_{-1} = 2000 min^{-1}; k_{+2} = 0.02 min^{-1}; k_{-2} = 0.004 min^{-1}.

Molecular modeling

Molecular dynamics of membrane systems with either the M_2 or M_3 receptor was run as described in Methods and analyzed with Desmond Simulation Interactions Diagram. In analysis of free molecular dynamics without methoctramine we focused on the o2 and o3 loops. Although in the crystal structure of the M_3 receptor (4DAJ) K523 forms a hydrogen bond with Y127 in the TM II (Fig. 9 top left), simulation of molecular dynamics shows that at 59 % of time K523 forms a hydrogen bond with the conserved glutamate E219 (Fig. 9 top right). In addition K523 binds to E219 by ionic interaction at 18 % of time and by water bridge at 21 % of time (Supplemental Figure 4 and 5). N419 at the M_2 receptor corresponds to K523 of M_3 receptor. The side chain of N419 is free in the M_2 crystal structure (Fig. 9 bottom left). Simulation of molecular dynamics indicated that N419 is free most of the time. This applies as well to E175 (corresponding residue to E219 in M_3 sequence) (Fig. 9 bottom right, Supplemental Figure 6 and 7).

In simulations of molecular dynamics of association of methoctramine with the M_2 receptor methoctramine was placed to extracellular vestibule by steered molecular dynamics. In continuing molecular dynamics simulations methoctramine nitrogen in atom position 10 forms a hydrogen bond with E175 at the o2 loop within first 30 ns (Fig. 10 left, Fig. 11 top, Supplemental Figure 8 and 11). After four cycles of alternating free and steered molecular dynamics (480 ns) the anisole group of methoctramine reached orthosteric binding site defined by D103 and N404. During subsequent free molecular dynamics methoctramine nitrogen in atom position 10 forms a hydrogen bond with D103, the anisole ring interacts with

Y104 in orthosteric site by π-π stacking interaction and methoctramine nitrogen in atom position 33 forms a hydrogen bond with E175 in o2 loop (Fig. 10 and 11 middle, Supplemental Figure 9 and 12). Two cycles of free molecular dynamics (total 240 ns) showed the methotramine anisole group moving towards TM VI to interact with Y403 by π-π stacking interaction and that the methoctramine oxygen in atom position 7 forms hydrogen bond with N404 (Fig. 10 right, Fig. 11 bottom, Supplemental Figure 10 and 13). Additionally methoctramine nitrogen in atom position 17 forms hydrogen bond with D103 in orthosteric binding site and nitrogen in atom position 33 forms hydrogen bond either with E172 or E175 in o2 loop (E172 59 % and E175 35 % of time).

Discussion

In this study we delineated the molecular mechanism of methoctramine (Fig. 1) binding and selectivity towards M_2 muscarinic receptors. We show that interaction of methoctramine with both the orthosteric and allosteric binding sites is responsible for its high-affinity at the M_2 receptor. Further we show that K523 in the third extracellular (o3) loop of the M_3 receptor interacts with E219 in the second extracellular (o2) loop and hinders interaction of methoctramine with the allosteric site, which results in low-affinity at the M_3 receptor.

Our results confirm earlier findings that in addition to the high-affinity competitive interaction with [^{3}H]NMS at the M_2 muscarinic receptors, methoctramine also binds to an allosteric domain on the M_2 muscarinic receptor. It has been noted that methoctramine slows-down [^{3}H]NMS dissociation from cardiac membranes (Giraldo et al., 1988; Waelbroeck, 1994) and that methoctramine noncompetitively inhibits carbachol-induced phosphoinositide hydrolysis (Lee et al., 1989) and left atria functional response to carbachol (Boselli and Grana, 1995). Our results directly demonstrate an allosteric feature of methoctramine binding at the M_2 receptor and its lack at M_3 receptors (Fig. 3).

To elucidate the amino acid residues involved in high affinity orthosteric and allosteric binding of methoctramine we genetically modified the M_3 receptors to resemble the M_2 receptors. We focused on the extracellular domains where allosteric ligands like alcuronium or gallamine (Krejčí and Tuček, 2001) have been proposed to bind to. We found that replacement of the whole o3 loop of the M_3 receptor with the corresponding sequence of the M_2 receptor increases the affinity of methoctramine and is thus responsible for high-affinity methoctramine binding. On the other hand, finding that this modification of the M_3 receptor does not influence the affinity of two other M_2 selective ligands, AF-DX 116 and himbacine,

and the M_3-selective ligand 4-DAMP (Table 1) proves that the o3 loop is not involved in M_2-selectivity in a general sense and means that different ligands gain their selectivity by interacting with different regions on receptor. Replacement of the o2 loop of the M_3 receptor by the o2 loop of the M_2 receptor does not influence the affinity of methoctramine. This mutation causes a decrease in affinity of the M_3-selective 4-DAMP, indicating involvement of the o2 loop in its high affinity for the M_3 receptor. These observations demonstrate that at least two additional domains exist which can determine ligand affinity besides the orthosteric site.

Sequence of the o3 loop of the M_2 and M_3 receptors differs in five positions (Supplemental Figure 3). Mutation of just K523 of the M_3 receptor to asparagine increases the affinity of methoctramine (Fig. 2) and uncovers allosteric properties of methoctramine, similar to those observed at the M_2 receptor (Fig. 4). Mutation K523N is thus sufficient for methoctramine binding to an allosteric site from which it slows down [^{3}H]NMS dissociation. We deduce that methoctramine interacts directly with the extracellular domain of the M_2 receptor and that this interaction is contingent on the presence of N419 in the o3 loop. This notion is further supported by the observation that the mutation M_2 P decreases affinity of the M_2 receptor for both [^{3}H]NMS and methoctramine (Table 2).

Equilibrium binding experiments on the M_3 receptor mutated at individual positions to corresponding amino acids of the M_2 sequence indicate that the double mutation of K523N and S519P is virtually sufficient to equalize the affinity of methoctramine at the mutated M_3 and the wild-type M_2 receptors (Fig. 2). The mutation S519P at the o3 loop of the M_3 receptor does not change affinity for methoctramine and does not reveal allosteric binding properties of methoctramine. These observations show that N419 of the M_2 receptor is solely required for methoctramine binding to the extracellular domain. However, N419 as well as P415 in the

o3 loop of the M_2 receptor are required for high affinity binding (Table 2).

Analysis of [^{3}H]NMS dissociation from the M_2 receptors in the presence of methoctramine shows that the rate of [^{3}H]NMS dissociation concentration-dependently decreases and approaches a limit of zero at concentrations above those necessary to saturate binding of methoctramine to its secondary allosteric binding site (Fig. 4). This demonstrates that, similar to other allosteric modulators (Proška and Tuček, 1994), methoctramine sterically prevents [^{3}H]NMS dissociation.

To gain insight into substructures involved in methoctramine high- and low-affinity binding, we tested interactions of two methoctramine precursors, the short and the long methoctramine precursors (SMP and LMP) (Fig. 1). Both precursors have lower affinity than methoctramine at the M_2 receptor whereas only SMP affinity was lower at the M_3 receptor (Table 2). Mutations in the o3 loop of the M_3 receptor affected the affinity of both methoctramine precursors in the same way as it modified the affinity of methoctramine. SMP possesses allosteric properties as evidenced by slowing-down of [^{3}H]NMS dissociation from the M_2 receptor and from the M_3K, M_3SK, and M_3DSKF mutants (Fig. 6, Table 3). The equilibrium dissociation constant of SMP binding to [^{3}H]NMS-occupied M_2 receptors is the same as of methoctramine indicating that this part of methoctramine molecule is sufficient for binding to the allosteric domain. The observed lower affinity of SMP than that of methoctramine under equilibrium binding to the M_2 receptor indicates that both parts of methoctramine molecule are involved in (needed for) methoctramine high-affinity binding.

FRET of binding kinetics of LMP at the M_2 receptors (Fig. 7) showed biphasic association as well as biphasic dissociation with proportion of slow dissociation increasing with time of association. These results are compatible with at least two receptor-ligand interaction models: 1/ isomerization of receptor-antagonist complex (Järv et al., 1979) and 2/ the tandem two-site

model (Jakubík et al., 2000). The same pattern of binding kinetics of LMP at the M_3 receptors (Fig. 8) can be observed. Much higher concentrations of LMP were required at M_3 receptors for the same effect as at M_2 receptors indicating dramatically lower affinity of LMP for the allosteric binding site at the M_3 than the M_2 receptors.

Simulations of molecular dynamics of methoctramine association with the M_2 receptor showed that binding is initiated by interaction with E175 at the o2 loop (Fig. 10 left) followed by slow translocation to the orthosteric binding site (Fig. 10 middle) and methoctramine binding equilibration (Fig. 10 right). Thus initial interaction with E175 (Fig. 11 top) represents the fast association step observed in FRET measurements (Fig. 7) and results in methoctramine low-affinity binding that prevents NMS dissociation. Slow translocation then represents the slow association step in FRET measurements (Fig. 7) and manifests itself as slowly dissociating sites whose proportion increases with time of association (proportion of occupied binding sites). Methoctramine interacts both with the orthosteric (D103, Y403, N404) and allosteric (E172, E175) sites (Fig. 11 bottom), and this dual interaction results in methoctramine high-affinity binding. As it is evident from molecular model (Fig. 10 middle and right, Fig. 11 middle and bottom) SMP is too short to interact with both sites and therefore has lower affinity than methoctramine. At the M_3 receptors methoctramine competes with K523 for interaction with E219 that is, unlike at the M_2 receptor, the only glutamate in the middle of the o2 loop and thus its binding to the allosteric site is impaired and contributes to low affinity of methoctramine binding at the M_3 receptors under equilibrium.

This work has practical implications. The major difficulty in producing muscarinic subtype-selective ligands is due to structurally conserved orthosteric binding site. Understanding the molecular mechanisms of methoctramine binding may be useful for designing a novel family of selective compounds that combine elements of known

high-affinity orthosteric ligands with known selective allosteric ligands in one molecule. Interaction of such hybrids with the orthosteric binding site would endow them with high-affinity while binding to the less conserved extracellular domain would give them subtype selectivity (Mohr et al., 2004; Antony et al., 2009). Modern methods using fluorescent ligands to detect ligand binding were described (Ilien etz al., 2003; Daval et al., 2012). Common problem with fluorescent labeling of ligands is that fluorescent probe alters ligand affinity. Presented results show that ligand affinity need not to be affected by fluorescent probe.

In summary, we demonstrate that the high-affinity methoctramine binding to the M_2 receptors is due to the simultaneous interaction with both the orthosteric and the allosteric binding sites. In orthosteric binding site methoctramine forms hydrogen bonds with D103 and N404, and interacts with Y403 via π-π stacking interaction. At the allosteric binding site methoctramine forms a hydrogen bond alternating between E172 and E175. Methoctramine can bind to the NMS occupied receptor with low affinity by interaction solely with the allosteric binding site. Although in such case the interaction between methoctramine and NMS is allosteric (is not mutually exclusive), NMS cannot leave the complex in the presence of methoctramine which physically prevents its dissociation. Lysine K523 in the o3 loop of the M_3 receptor interacts with E219 in the o2 loop and hinders methoctramine binding to the allosteric site. It results in low affinity of methoctramine binding and lack of allosteric properties at the M_3 receptors.

Authorship Contributions

Participated in research design: Jakubík, El-Fakahany, Doležal

Conducted experiments: Jakubík, Zimčík, Randáková

Contributed new reagents: Fuksová

Performed data analysis: Jakubík, Doležal

Wrote or contributed to the writing of the manuscript: Jakubík, El-Fakahany, Doležal

References

Antony J, Kellershohn K, Mohr-Andrä M, Kebig A, Prilla S, Muth M, Heller E, Disingrini T, Dallanoce C, Bertoni S, Schrobang J, Tränkle C, Kostenis E, Christopoulos A, Höltje H, Barocelli E, De Amici M, Holzgrabe U and Mohr K (2009) Dualsteric GPCR targeting: a novel route to binding and signaling pathway selectivity. *FASEB J* **23**: 442-450.

Bonner TI, Buckley NJ, Young AC and Brann MR (1987) Identification of a family of muscarinic acetylcholine receptor genes. *Science* **237**: 527-532.

Bonner TI (1989) The molecular basis of muscarinic receptor diversity. *Trends Neurosci* **12**: 148-151.

Boselli C and Grana E (1995) Mode of antagonism of methoctramine, AF-DX 116 and hexahydrosiladifenidol in guinea-pig left atrium and ileum: comparison of Schild and resultant analysis. *J Auton Pharmacol* **15**: 115-127.

Bowers KJ, Chow E, Xu H, Dror RO, Eastwood MP, Gregersen BA, Klepeis JL, Kolossvary I, Moraes MA, Sacerdoti FD, Salmon JK, Shan Y, Shaw DE (2006) Scalable algorithms for molecular dynamics simulations on commodity clusters. In: Proceedings of the ACM/IEEE conference on supercomputing (SC06), Article No. 84.

Caulfield MP (1993) Muscarinic receptors--characterization, coupling and function. *Pharmacol Ther* **58**: 319-379.

Christopoulos A, Pierce TL, Sorman JL and El-Fakahany EE (1998) On the unique binding and activating properties of xanomeline at the M1 muscarinic acetylcholine receptor. *Mol Pharmacol* **53**: 1120-1130.

Daval SB, Valant C, Bonnet D, Kellenberger E, Hibert M, Galzi J and Ilien B (2012) Fluorescent derivatives of AC-42 to probe bitopic orthosteric/allosteric binding mechanisms on muscarinic M1 receptors. *J Med Chem* **55**: 2125-2143.

Giraldo E, Micheletti R, Montagna E, Giachetti A, Viganò MA, Ladinsky H and Melchiorre C (1988) Binding and functional characterization of the cardioselective muscarinic antagonist methoctramine. *J Pharmacol Exp Ther* **244**: 1016-1020.

Gnagey AL, Seidenberg M and Ellis J (1999) Site-directed mutagenesis

reveals two epitopes involved in the subtype selectivity of the allosteric interactions of gallamine at muscarinic acetylcholine receptors. *Mol Pharmacol* **56**: 1245-1253.

Haga K, Kruse AC, Asada H, Yurugi-Kobayashi T, Shiroishi M, Zhang C, Weis WI, Okada T, Kobilka BK, Haga T and Kobayashi T (2012) Structure of the human M_2 muscarinic acetylcholine receptor bound to an antagonist. *Nature* **482**: 547-551.

Hoops S, Sahle S, Gauges R, Lee C, Pahle J, Simus N, Singhal M, Xu L, Mendes P and Kummer U (2006) COPASI--a COmplex PAthway SImulator. *Bioinformatics* **22**: 3067-3074.

Ilien B, Franchet C, Bernard P, Morisset S, Weill CO, Bourguignon J, Hibert M and Galzi J (2003) Fluorescence resonance energy transfer to probe human M_1 muscarinic receptor structure and drug binding properties. *J Neurochem* **85**: 768-778.

Jakubík J and Tuček S (1994) Two populations of muscarinic binding sites in the chick heart distinguished by affinities for ligands and selective inactivation. *Br J Pharmacol* **113**: 1529-1537.

Jakubík J, Bačáková L, el-Fakahany EE and Tuček S (1995) Constitutive activity of the M_1-M_4 subtypes of muscarinic receptors in transfected CHO cells and of muscarinic receptors in the heart cells revealed by negative antagonists. *FEBS Lett* **377**: 275-279.

Jakubík J, El-Fakahany EE and Tuček S (2000) Evidence for a tandem two-site model of ligand binding to muscarinic acetylcholine receptors. *J Biol Chem* **275**: 18836-18844.

Jakubík J, Krejčí A and Doležal V (2005) Asparagine, valine, and threonine in the third extracellular loop of muscarinic receptor have essential roles in the positive cooperativity of strychnine-like allosteric modulators. *J Pharmacol Exp Ther* **313**: 688-696.

Järv J, Hedlund B and Bartfai T (1979) Isomerization of the muscarinic receptor . antagonist complex. *J Biol Chem* **254**: 5595-5598.

Krejčí A and Tuček S (2001) Changes of cooperativity between N-methylscopolamine and allosteric modulators alcuronium and gallamine induced by mutations of external loops of muscarinic M_3 receptors. *Mol Pharmacol* **60**: 761-767.

Kruse AC, Hu J, Pan AC, Arlow DH, Rosenbaum DM, Rosemond E, Green HF, Liu T, Chae PS, Dror RO, Shaw DE, Weis WI, Wess J and Kobilka BK (2012) Structure and dynamics of the M_3 muscarinic acetylcholine receptor. *Nature* **482**: 552-556.

Lazareno S and Birdsall NJ (1995) Detection, quantitation, and verification of allosteric interactions of agents with labeled and unlabeled ligands at G protein-coupled receptors: interactions of strychnine and acetylcholine at muscarinic receptors. *Mol Pharmacol* **48**: 362-378.

Lee NH, Fryer AD, Forray C and el-Fakahany EE (1989) Different mechanisms of antagonism by methoctramine of two neuronal muscarinic receptor-mediated second messenger responses. *J Pharmacol Exp Ther* **251**: 992-999.

Leppik RA, Miller RC, Eck M and Paquet JL (1994) Role of acidic amino acids in the allosteric modulation by gallamine of antagonist binding at the m2 muscarinic acetylcholine receptor. *Mol Pharmacol* **45**: 983-990.

Matsui H, Lazareno S and Birdsall NJ (1995) Probing of the location of the allosteric site on m1 muscarinic receptors by site-directed mutagenesis. *Mol Pharmacol* **47**: 88-98.

Melchiorre C, Cassinelli A and Quaglia W (1987) Differential blockade of muscarinic receptor subtypes by polymethylene tetraamines. Novel class of selective antagonists of cardiac M-2 muscarinic receptors. *J Med Chem* **30**: 201-204.

Melchiorre C, Minarini A, Angeli P, Giardinà D, Gulini U and Quaglia W (1989) Polymethylene tetraamines as muscarinic receptor probes. *Trends Pharmacol Sci* **Suppl**: 55-59.

Mohr M, Heller E, Ataie A, Mohr K and Holzgrabe U (2004) Development of a new type of allosteric modulator of muscarinic receptors: hybrids of the antagonist AF-DX 384 and the hexamethonio derivative W84. *J Med Chem* **47**: 3324-3327.

Proška J and Tuček S (1994) Mechanisms of steric and cooperative actions of alcuronium on cardiac muscarinic acetylcholine receptors. *Mol Pharmacol* **45**: 709-717.

Tuček S and Proška J (1995) Allosteric modulation of muscarinic acetylcholine receptors. *Trends Pharmacol Sci* **16**: 205-212.

Waelbroeck M (1994) Identification of drugs competing with d-tubocurarine for an allosteric site on cardiac muscarinic receptors. *Mol Pharmacol* **46**: 685-692.

Wess J (1996) Molecular biology of muscarinic acetylcholine receptors. *Crit Rev Neurobiol* **10**: 69-99.

Footnotes

This work was supported by the Academy of Sciences of the Czech Republic project [AV0Z 50110509] and support [RVO:67985823], the Grant Agency of the Czech Republic grants [305/09/0681] and [P304/12/G069].

Legends to figures

Fig. 1

Structutres of methoctramine and its precursors.

Top, methoctramine, 1,26-bis(2-methoxyphenyl)-2,9,18,25-tetraazahexacosane; middle, short methoctramine precursor (SMP), 6-aminohexyl)[(2-methoxyphenyl)methyl]amine; bottom, long methoctramine precursor (LMP), 8-amino-N-(6-{[(2-methoxyphenyl)methyl]amino}hexyl)octanamide. For the synthesis of precursors see Supplemental Figure 1.

Fig. 2

Inhibition of [^{3}H]NMS binding to M_2, M_3 and mutant M_3 receptors by methoctramine.

Binding of [^{3}H]NMS to membranes expressing wild type M_2 or M_3 or mutant M_3 receptors was measured at increasing concentrations of methoctramine. Binding is expressed as percentage of [^{3}H]NMS binding to the membranes incubated in the absence of methoctramine (950 through 2300 dpm). Data are means ± S.E.M. of 4 to 6 independent experiments performed in quadruplicates. For the mutants nomenclature see Methods and Supplemental Figure 3.

Fig. 3

Effects of methoctramine on the dissociation of [^{3}H]NMS from M_2 (top) or M_3 (bottom) receptors.

Membranes expressing wild type M_2 (top) or M_3 (bottom) receptors were preincubated for 1 hour with 750 pM [^{3}H]NMS. The dissociation was started at time 0 on the x-axis by the

addition of unlabeled NMS to a final concentration of 1 μM. Unlabeled NMS was added either alone (closed squares) or in mixture with methoctramine. The final concentration of methoctramine was either 10 μM (hatched squares) or 100 μM (open squares). Data are means ± S.E.M. of 3 to 4 independent experiments performed in quadruplicates. Parameters of fits are listed in Table 3.

Fig. 4

Dependence of the dissociation rate of [^{3}H]NMS from M_2 and M_3 wild-type and mutated M_3 receptors on the concentration of methoctramine.

Observed rate dissociation constants ($k_{off(obs)}$) obtained by nonlinear regression analysis of dissociation curves similar to those shown in Fig. 3 are plotted against the concentrations of methoctramine. Curves are the result of fitting Eq. 5 to the data. Fitting parameters are shown in Table 3. Data are means ± S.E.M. of 3 to 4 independent experiments performed in quadruplicates. For the mutants nomenclature see Methods and Supplemental Figure 3.

Fig. 5

Inhibition of [^{3}H]NMS binding to M_2, M_3 and mutant M_3 receptors by short and long methoctramine precursors.

Binding of [^{3}H]NMS to membranes expressing wild type M_2 or M_3 or mutant M_3 receptors was measured at increasing concentrations of short methoctramine precursor (SMP, top), and long methoctramine precursor (LMP, bottom). Binding is expressed as percentage of [^{3}H]NMS binding to the membranes incubated in the absence of methoctramine precursors (1100 through 2200 dpm). Data are means ± S.E.M. of 4 independent experiments performed in quadruplicates. Parameters of fits are listed in Table 2. For the mutants nomenclature see

Methods and Supplemental Figure 3.

Fig. 6

Dependence of the dissociation rate of [^{3}H]NMS from M_2 and M_3 wild-type and mutated M_3 receptors on the concentration of the short methoctramine precursor (SMP).

Observed rate dissociation constants ($k_{off(obs)}$) obtained by nonlinear regression analysis of dissociation curves like in Fig. 3 are plotted against concentration of SMP. Curves are result of fitting Eq. 5 to the data. Parameters are shown in Table 3. Data are means ± S.E.M. of 3 independent experiments performed in quadruplicates. For the mutants nomenclature see Methods and Supplemental Figure 3.

Fig. 7

Kinetics of FRET signal between GFP-M_2 receptor and Alexa-555-LMP.

Time course of association (black) and dissociation initiated after 5 (red), 60 (green) and 120 min (blue) of association of 30 (top), 100 (middle) and 300 nM (bottom) Alexa-555-LMP with GFP-M_2 receptors. Emission of Alexa-555-LMP at 590 nm after excitation of GFP-M_2 receptors at 470 nm is expressed in arbitrary units after correction for bleaching. Data are means ± S.E.M. of 3 independent experiments performed in duplicates. Parameters of fits are listed in Supplemental Data Table S2.

Fig. 8

Kinetics of FRET between GFP-M_3 receptor and Alexa-555-LMP.

Time course of association (black) and dissociation initiated after 60 (green), 120 (blue) and 240 min (yellow) of association of 100 (top), 300 (middle) and 1000 nM (bottom)

Alexa-555-LMP with GFP-M_3 receptors. Emission of Alexa-555-LMP at 590 nm after excitation of GFP-M_3 receptors at 470 nm is expressed in arbitrary units after correction for bleaching. Data are means ± S.E.M. of 3 independent experiments performed in duplicates. Parameters of fits are listed in Supplemental Data Table S3.

Fig. 9

Interaction of K522 at M_3 receptor and lack of interaction of corresponding N419 in M_2 receptor.

Extracellular view of initial structures (left) and average structures (right) of simulation of free molecular dynamics of M_3 (top) and M_2 (bottom) receptors. Red – TM II, white – o2 loop, blue – o3 loop and TM VII, yellow – hydrogen bond. Elements: cyan – carbon, red – oxygen, blue – nitrogen, white – hydrogen.

Fig. 10

Simulation of molecular dynamic of methoctramine association with M_2 receptors.

Three stages of molecular dynamics are displayed: Initial (left), transient (middle) and final (right). Extracellular part of the M_2 receptor is up and TM IV and V are in front. Backbone of the receptor is colored by position in red to white to blue gradient. Side chains of D103, E172, E175, N404 and Y430 are displayed. Cyan - carbon, blue – nitrogen, green – carbon of methoctramine, red – oxygen; yellow – hydrogen bonds. For high-resolution graphics see Supplemental Figure 8, 9 and 10.

Fig. 11

Ligand interaction diagrams of molecular dynamic simulation of methoctramine association

with the M_2 receptor.

Ligand interaction diagrams of initial (top), transient (middle) and final (bottom) stage of association are shown. Grey – solvent exposure, red – charged, blue – polar, green – hydrophobic, dotted arrow – H-bond to side chain, full arrow – H-bond to backbone, green connector – π-π stacking. For high-resolution graphics see Supplemental Figure 11, 12 and 13.

Tables

Table 1

Inhibition constants of selective muscarinic ligands for wild type M_2 and M_3, and hybrid $M_3(o2M_2)$ and $M_3(o3M_2)$ receptors.

Negative logarithms of inhibition constants (pK_i) were obtained by nonlinear regression of data from competition experiments of antagonist vs. [^{3}H]NMS. Eq. 2 was fitted to the data to obtain IC_{50}. K_i was computed according Eq. 3. Data are means ± S.E.M. from 4 independent experiments.

	M_2	M_3	$M_3(o2M_2)$	$M_3(o3M_2)$
4-DAMP	7.72 ± 0.06	8.50 ± 0.09	6.84 ± 0.05*	8.35 ± 0.07
AF-DX 116	7.18 ± 0.04	5.68 ± 0.05	5.54 ± 0.05	5.68 ± 0.06
Himbacine	7.56 ± 0.08	6.93 ± 0.03	6.83 ± 0.08	6.91 ± 0.06
Methoctramine	7.29 ± 0.04	5.69 ± 0.12	5.89 ± 0.11	7.17 ± 0.04*

*, Significantly different from wild-type M_3 ($p < 0.01$ by Student's two-tailed t test).

Table 2

Binding parameters of wild type M_2 and M_3 and mutated M_3 receptors.

Values of equilibrium dissociation constants (K_d) were obtained by nonlinear regression analysis of saturation binding experiments. Values of negative logarithms of methoctramine inhibition constants (pK_i) were obtained by nonlinear regression of data shown in Figs. 2 and 5. Eq. 2 was fitted to the data to obtain IC_{50}. K_i was computed according Eq. 3. Data are means ± S.E.M. from 4 to 6 independent experiments performed in quadruplicates.

Receptor ¶	[^{3}H]NMS K_d [nM]	methoctramine pK_i	SMP pK_i	LMP pK_i
M_3 wt	0.32 ± 0.01	5.69 ± 0.12	4.41 ± 0.15	5.43 ± 0.13
M_2 wt	0.78 ± 0.04	7.29 ± 0.04	5.25 ± 0.12	6.78 ± 0.08
Mutations in o3 of M_3				
M_3 S	0.32 ± 0.02[a]	5.95 ± 0.15[a,b]	4.58 ± 0.14[a]	5.64 ± 0.12
M_3 K	0.34 ± 0.02[a]	6.49 ± 0.11[*,a]	4.96 ± 0.15[*,a]	6.15 ± 0.11[*,a]
M_3 KFN	0.51 ± 0.03[*,a]	6.51 ± 0.09[*,a]	n.d.	n.d.
M_3 DKFN	0.49 ± 0.03[*,a]	6.51 ± 0.16[*,a]	n.d.	n.d.
M_3 SK	0.34 ± 0.02[a]	7.02 ± 0.19[*,b]	5.33 ± 0.09[*]	6.65 ± 0.09[*]
M_3 SKFN	0.68 ± 0.05[*]	7.04 ± 0.15[*,b]	n.d.	n.d.
M_3 DSKFN	0.76 ± 0.05[*]	7.17 ± 0.04[*,b]	5.20 ± 0.11[*]	6.68 ± 0.08[*]
Mutations in o3 of M_2				
M_2 P	0.62 ± 0.05[a]	6.31 ± 0.12[a]	n.d.	n.d.

¶, for the mutants nomenclature see Methods and Supplemental Figure 3. Significantly different from M_3 wt ([*]), M_2 wt ([a]) or M_3 K ([b]) ($p < 0.01$, Multiparametric one-way ANOVA with Tukey-Kramer post-test). n.d., not determined.

Table 3

Effect of methoctramine on [^{3}H]NMS dissociation.

Observed rate dissociation constants ($k_{off(obs)}$) of [^{3}H]NMS binding in the absence or presence of 100 µM methoctramine were obtained by nonlinear regression analysis of dissociation experiments shown in Fig. 3 using Eq. 4. Values of apparent equilibrium dissociation constant (K_D) for methoctramine and SMP were obtained by fitting Eq. 5 to the data in Fig. 4 and 6, respectively. Data are means ± S.E.M. form 3 to 5 independent experiments.

Receptor ¶	NMS $K_{off(obs)}$[min^{-1}]			methoctramine		SMP	
	control	methoctramine	SMP	ratio	pK_D	ratio	pK_D
M_3 wt	0.053 ± 0.002	0.046 ± 0.003	0.046 ± 0.004	1.1 ± 0.2	n.c.	1.1 ± 0.2	n.c.
M_2 wt	0.33 ± 0.01	0.0062 ± 0.0002	0.0096 ± 0.0005	53 ± 4	5.55 ± 0.05	34 ± 2	5.52 ± 0.04
Mutations in o3 of M_3							
M_3 S	0.070 ± 0.004[a]	0.047 ± 0.004[a]	0.047 ± 0.005	1.5 ± 0.2[a]	< 4[a]	1.5 ±0.2	< 4[a]
M_3 K	0.12 ± 0.01[*,a]	0.016 ± 0.001[*,a]	0.017 ± 0.002	7.5 ± 0.9[a]	5.11 ± 0.09	7.1 ± 0.4	5.0 ± 0.1
M_3 KFN	0.32 ± 0.01[*]	0.018 ± 0.003[*,a]	n.d.	17 ± 3[*,a]	5.12 ± 0.03	n.c.	n.c.
M_3 DKFN	0.26 ± 0.01[*,a]	0.013 ± 0.003[*]	n.d.	20 ± 4[*,a]	5.14 ± 0.06	n.c.	n.c.

Receptor ¶	NMS $K_{off(obs)}$[min^{-1}]			methoctramine		SMP	
M_3 SK	0.15 ± 0.01^{*,a}	0.012 ± 0.002*	0.013 ± 0.002	13 ± 3^{a}	5.23 ± 0.09	12 ± 2	5.13 ± 0.08
M_3 SKFN	0.31 ± 0.02*	0.0097 ± 0.0005*	n.d.	32 ± 4*	5.24 ± 0.05	n.c.	n.c.
M_3 DSKFN	0.32 ± 0.01*	0.0084 ± 0.0003*	0.0085 ± 0.0007	38 ± 3*	5.29 ± 0.04	38 ± 2	5.29 ± 0.03
Mutations in o3 of M_2							
M_2 P	0.27 ± 0.02*	0.012 ± 0.002*	n.d.	23 ± 6^{*,a}	5.49 ± 0.05	n.c.	n.c.

¶, for the mutants nomenclature see Methods and Supplemental Figure 3. n.c., not calculated; n.d., not determined. Significantly different from M_3 wt (*) or M_2 wt (^{a}) ($p < 0.01$ by multiparametric one-way ANOVA with Tukey-Kramer post-test). For more statistical analysis see Results.

Fig. 1

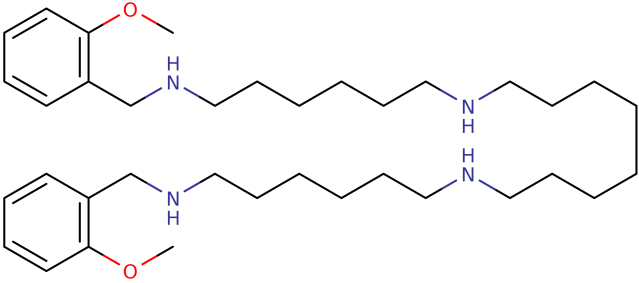

methoctramine

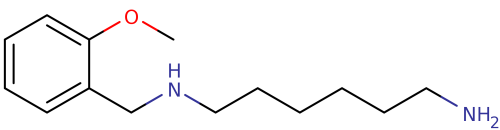

SMP

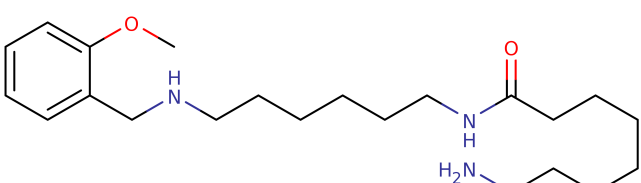

LMP

Fig. 2

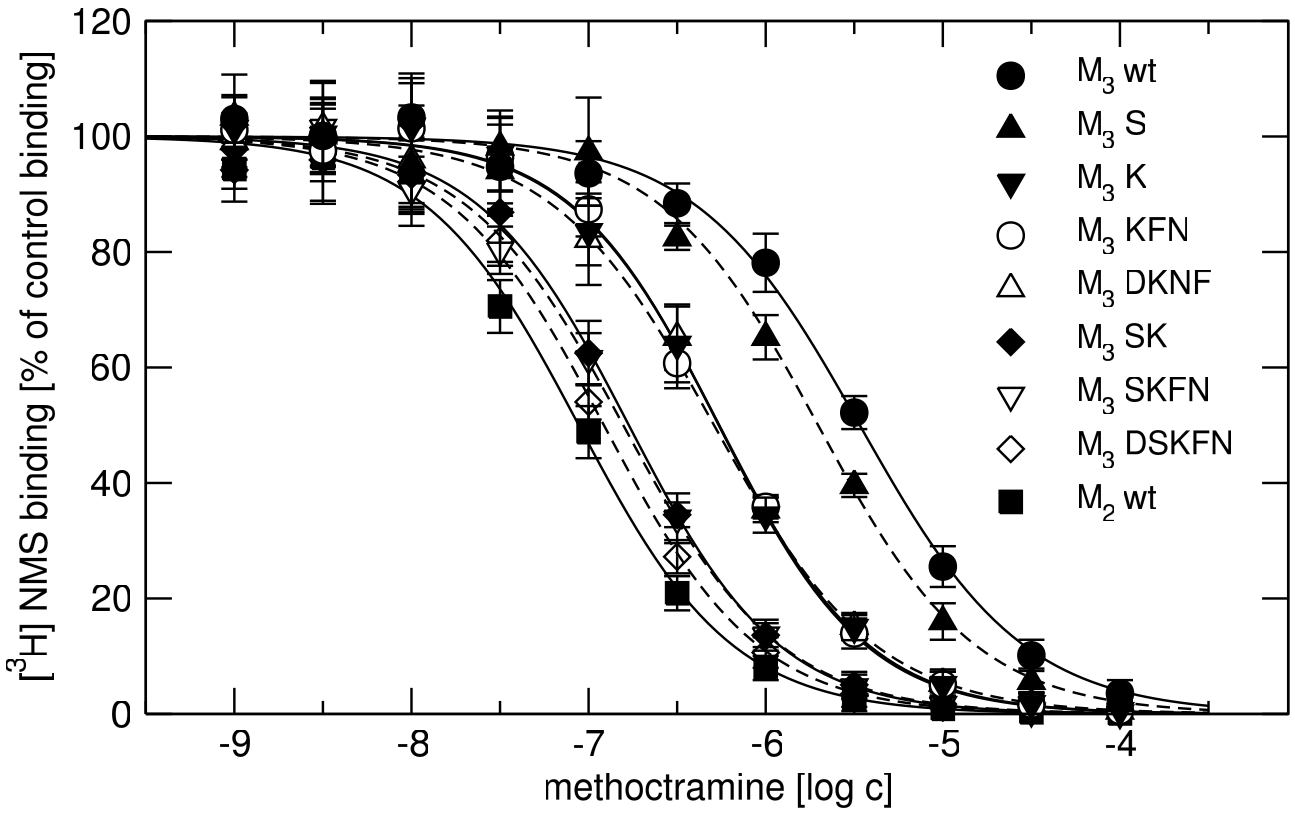
120
100
80
60
40
20
0
[3H] NMS binding [% of control binding]
-9
-8
-7
-6
-5
-4
methoctramine [log c]
M3 wt
M3 S
M3 K
M3 KFN
M3 DKNF
M3 SK
M3 SKFN
M3 DSKFN
M2 wt

Fig. 3

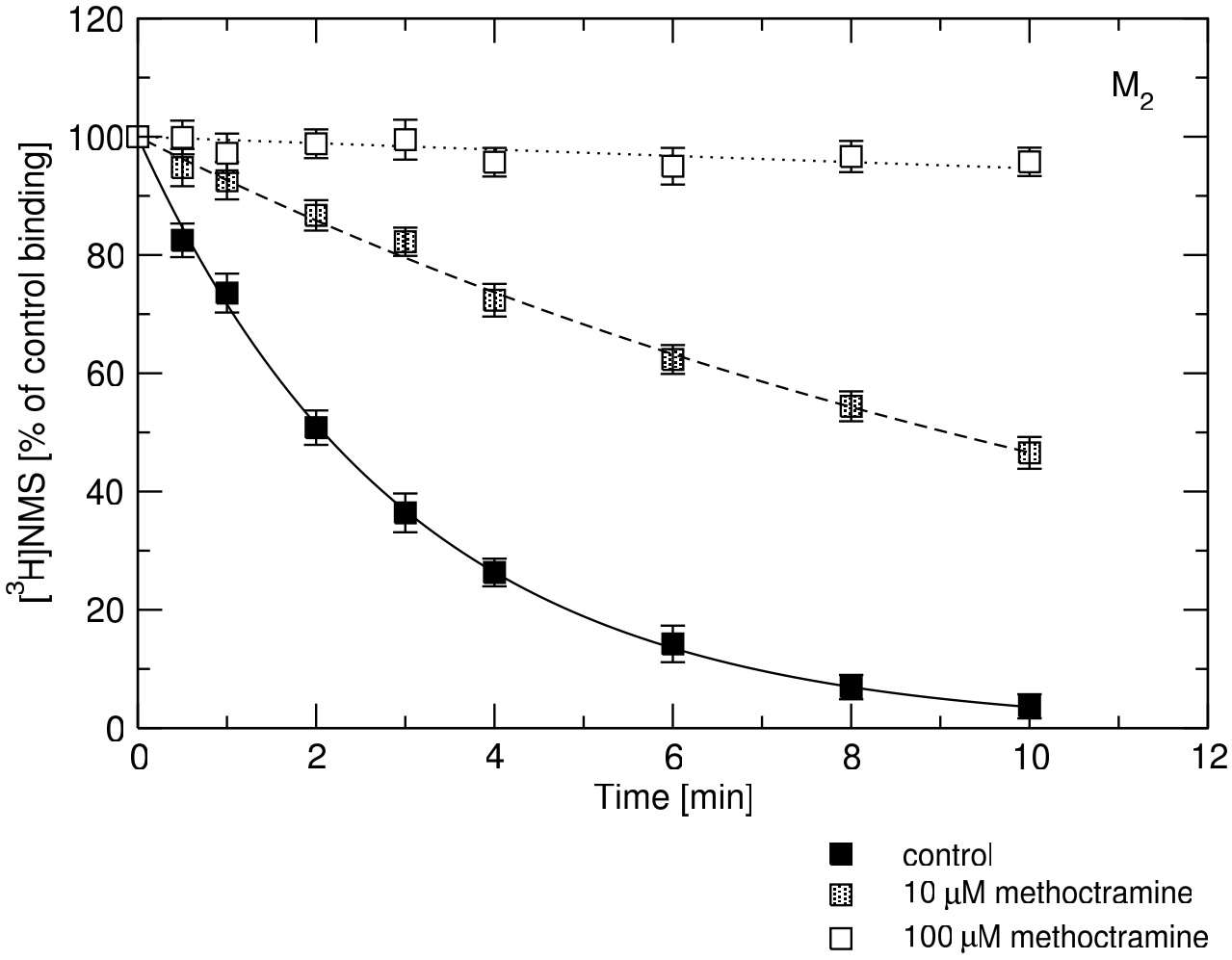
M2
[3H]NMS [% of control binding]
Time [min]
control
10 µM methoctramine
100 µM methoctramine

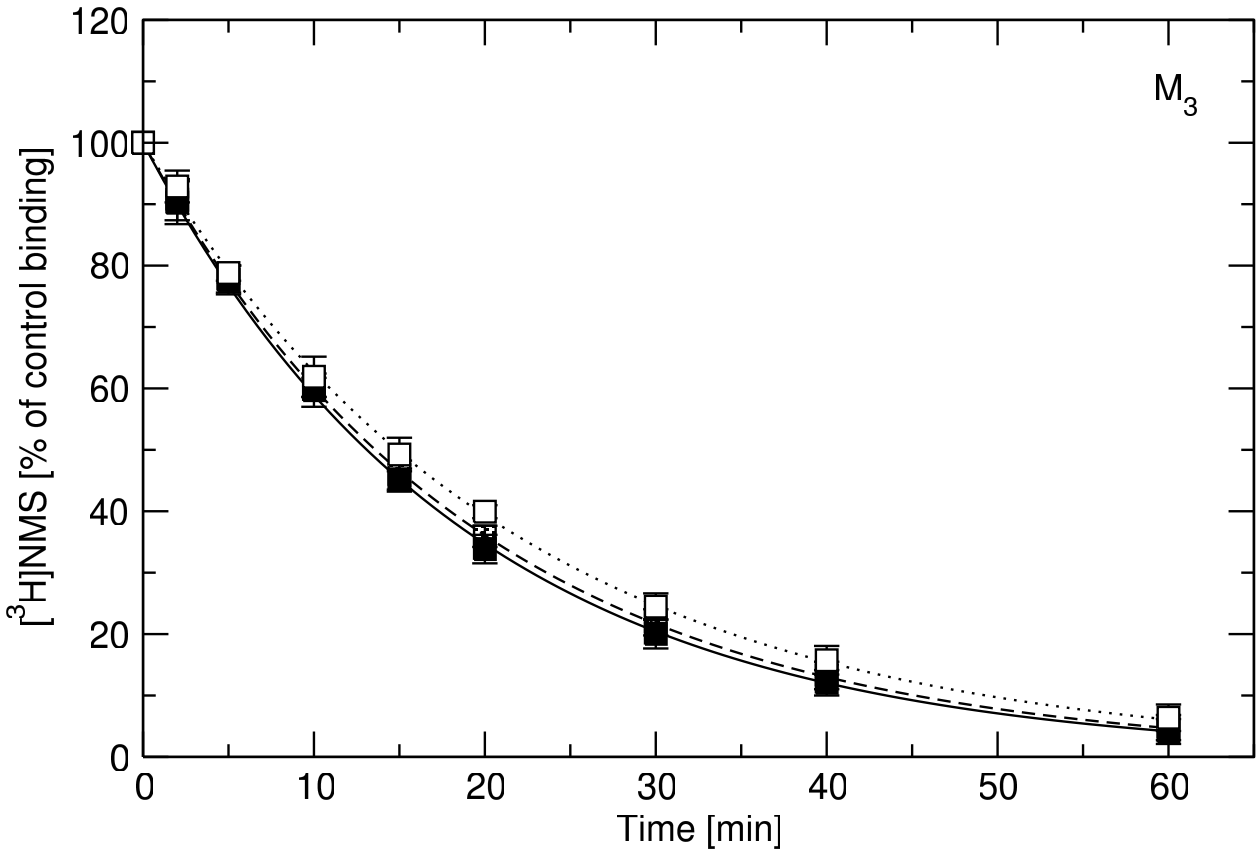
M3
[3H]NMS [% of control binding]
Time [min]

Fig. 4

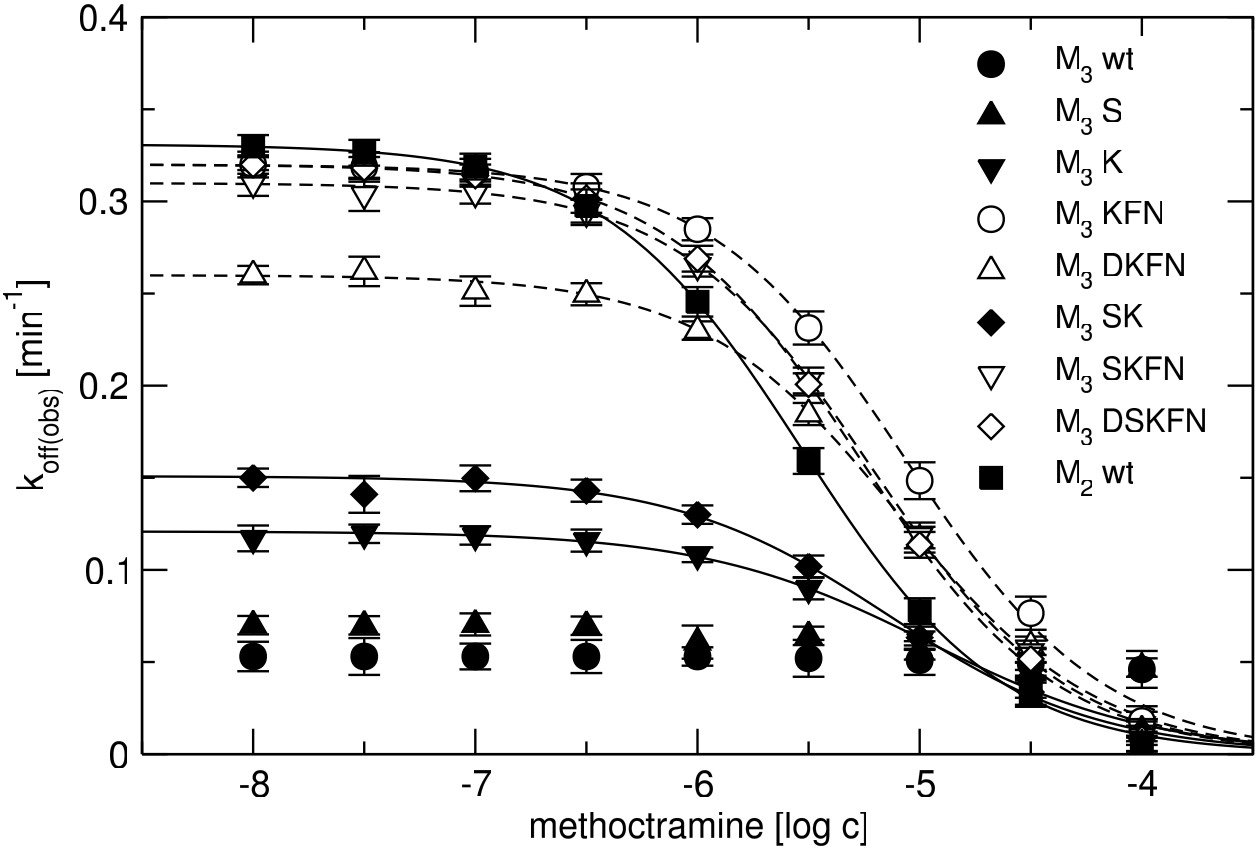
0.4
0.3
0.2
0.1
0
$k_{off(obs)}$ [min^{-1}]
-8
-7
-6
-5
-4
methoctramine [log c]
M_3 wt
M_3 S
M_3 K
M_3 KFN
M_3 DKFN
M_3 SK
M_3 SKFN
M_3 DSKFN
M_2 wt

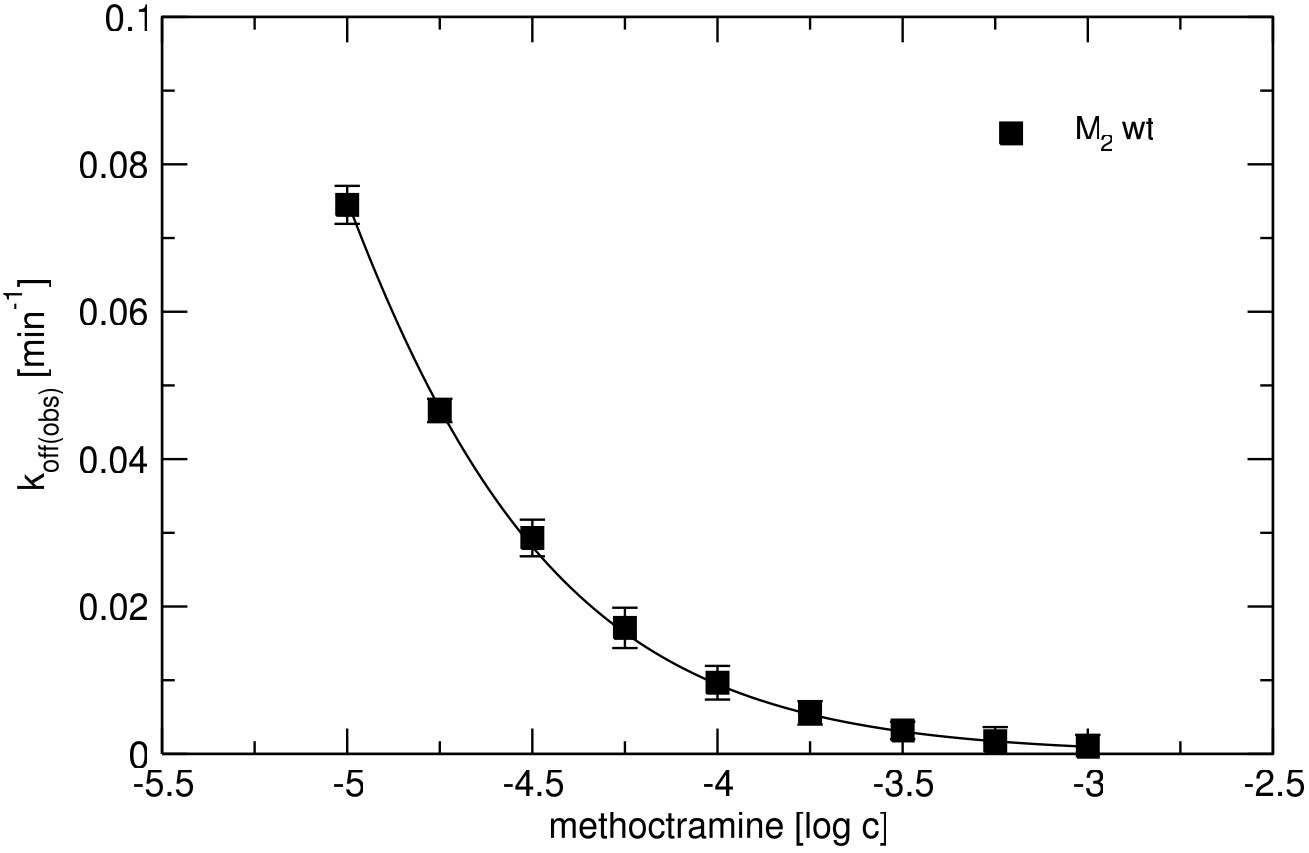
0.1
0.08
0.06
0.04
0.02
0
$k_{off(obs)}$ [min^{-1}]
-5.5
-5
-4.5
-4
-3.5
-3
-2.5
methoctramine [log c]
M_2 wt

Fig. 5

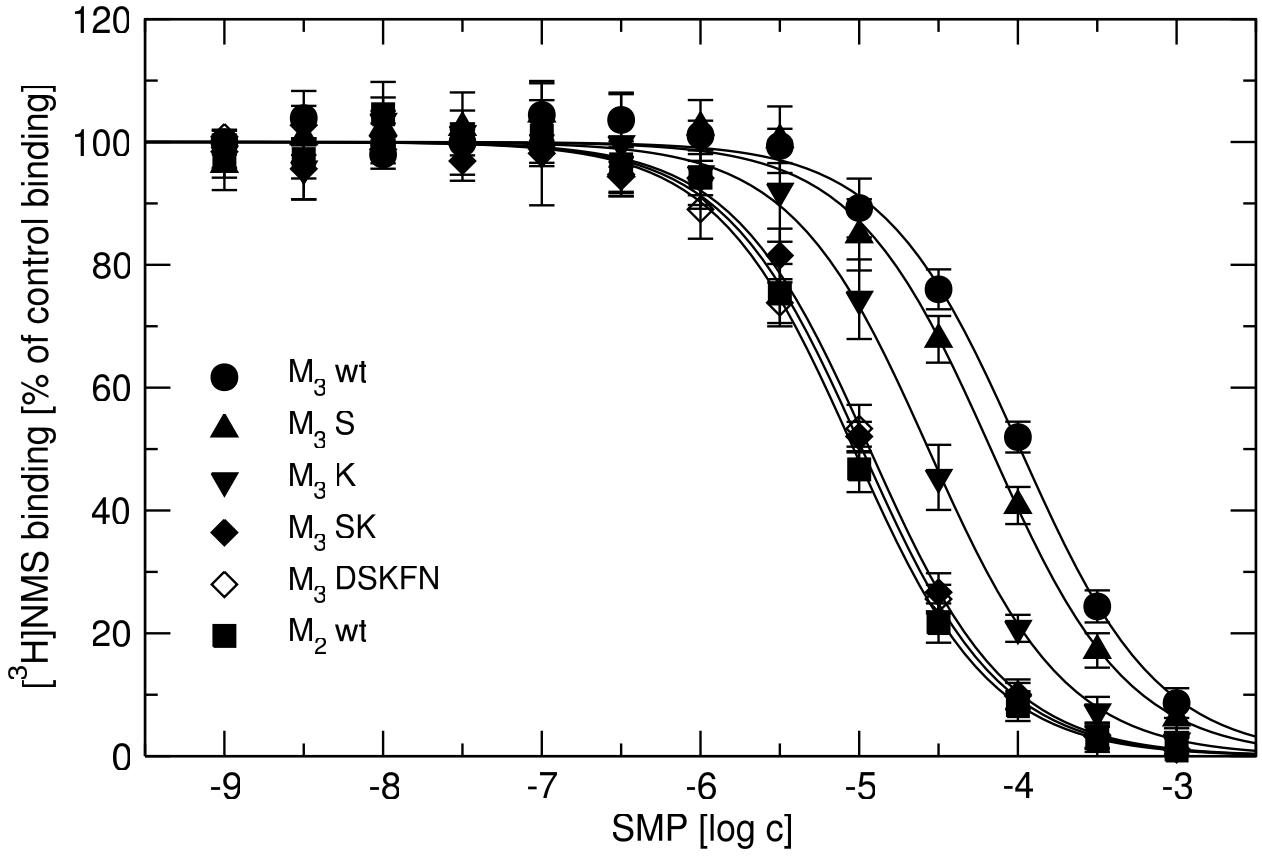
120
100
80
60
40
20
0
[3H]NMS binding [% of control binding]
M3 wt
M3 S
M3 K
M3 SK
M3 DSKFN
M2 wt
-9
-8
-7
-6
-5
-4
-3
SMP [log c]

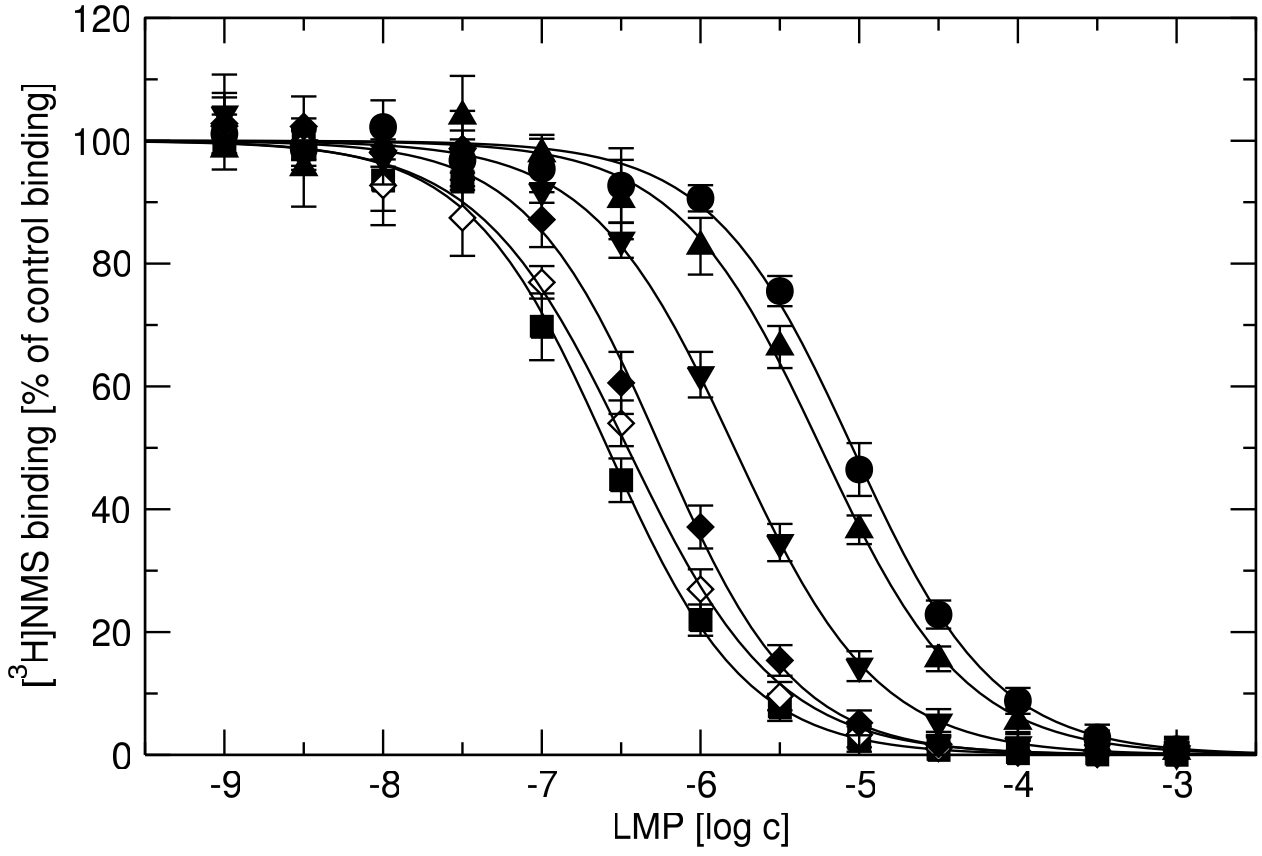
120
100
80
60
40
20
0
[3H]NMS binding [% of control binding]
-9
-8
-7
-6
-5
-4
-3
LMP [log c]

Fig. 6

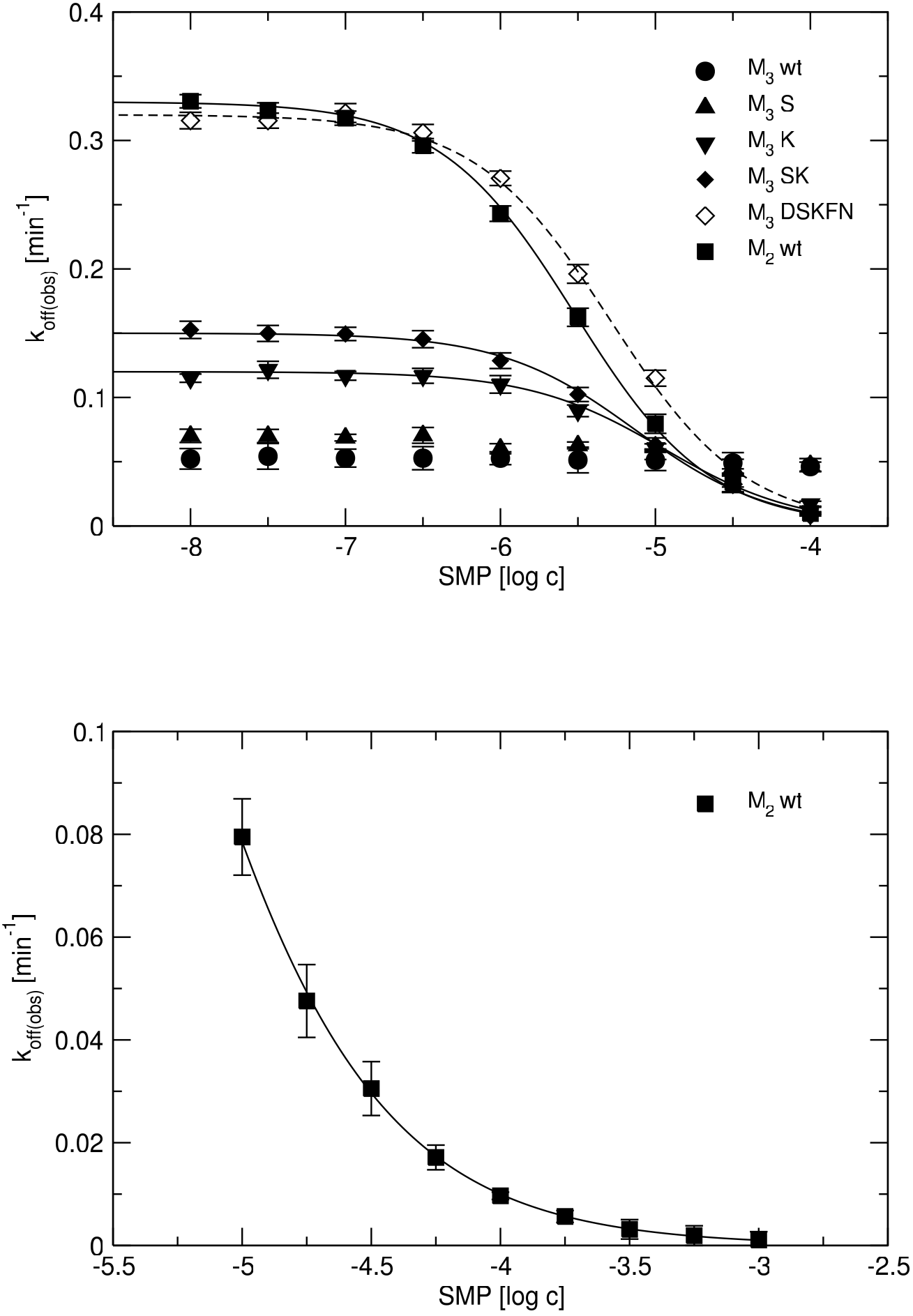
0.4
0.3
0.2
0.1
0
$k_{off(obs)}$ [min^{-1}]
-8
-7
-6
-5
-4
SMP [log c]
M_3 wt
M_3 S
M_3 K
M_3 SK
M_3 DSKFN
M_2 wt
0.1
0.08
0.06
0.04
0.02
0
$k_{off(obs)}$ [min^{-1}]
-5.5
-5
-4.5
-4
-3.5
-3
-2.5
SMP [log c]
M_2 wt

Fig. 7

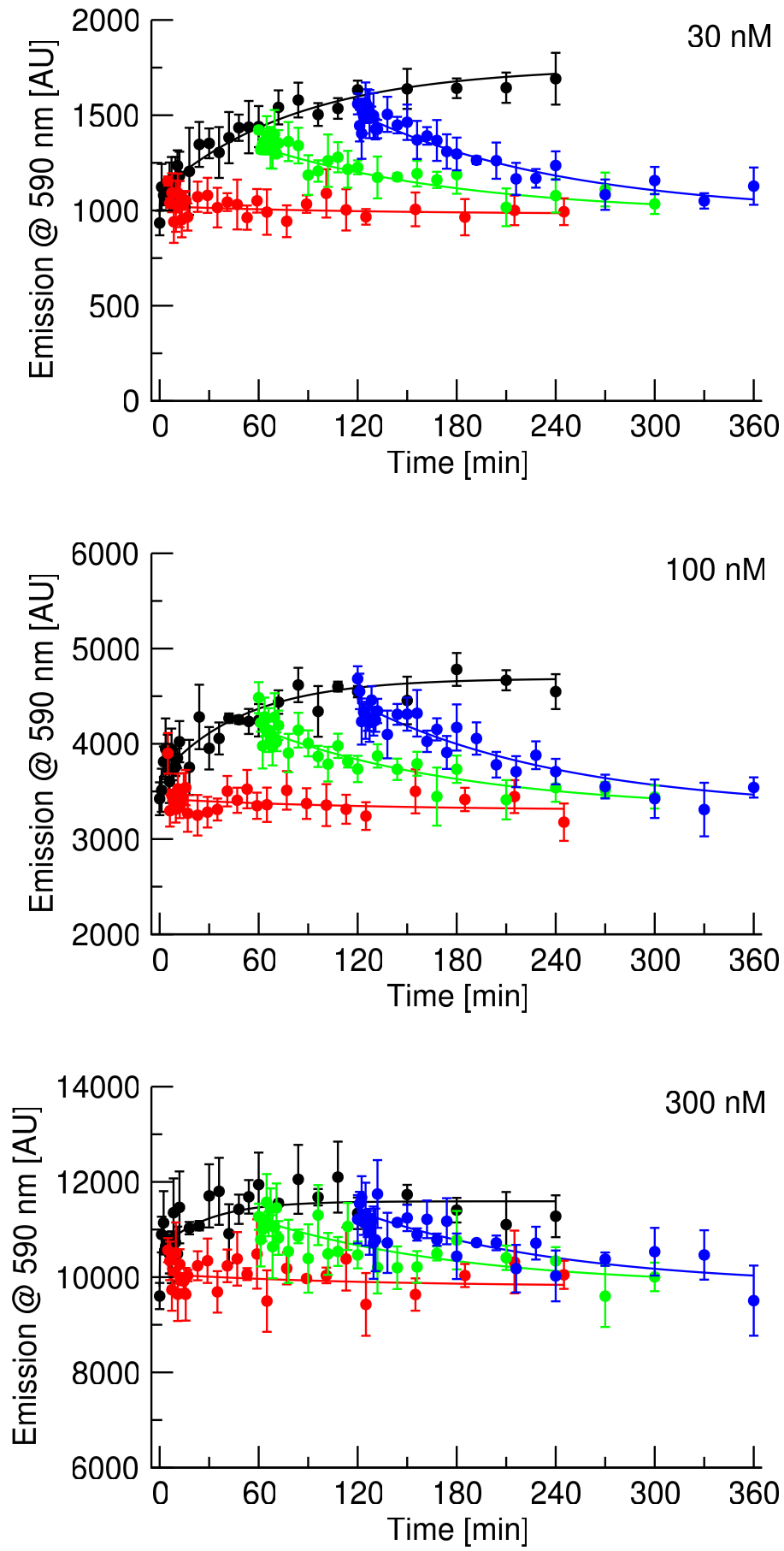
30 nM
Emission @ 590 nm [AU]
2000
1500
1000
500
0
0
60
120
180
240
300
360
Time [min]
100 nM
Emission @ 590 nm [AU]
6000
5000
4000
3000
2000
0
60
120
180
240
300
360
Time [min]
300 nM
Emission @ 590 nm [AU]
14000
12000
10000
8000
6000
0
60
120
180
240
300
360
Time [min]

Fig. 8

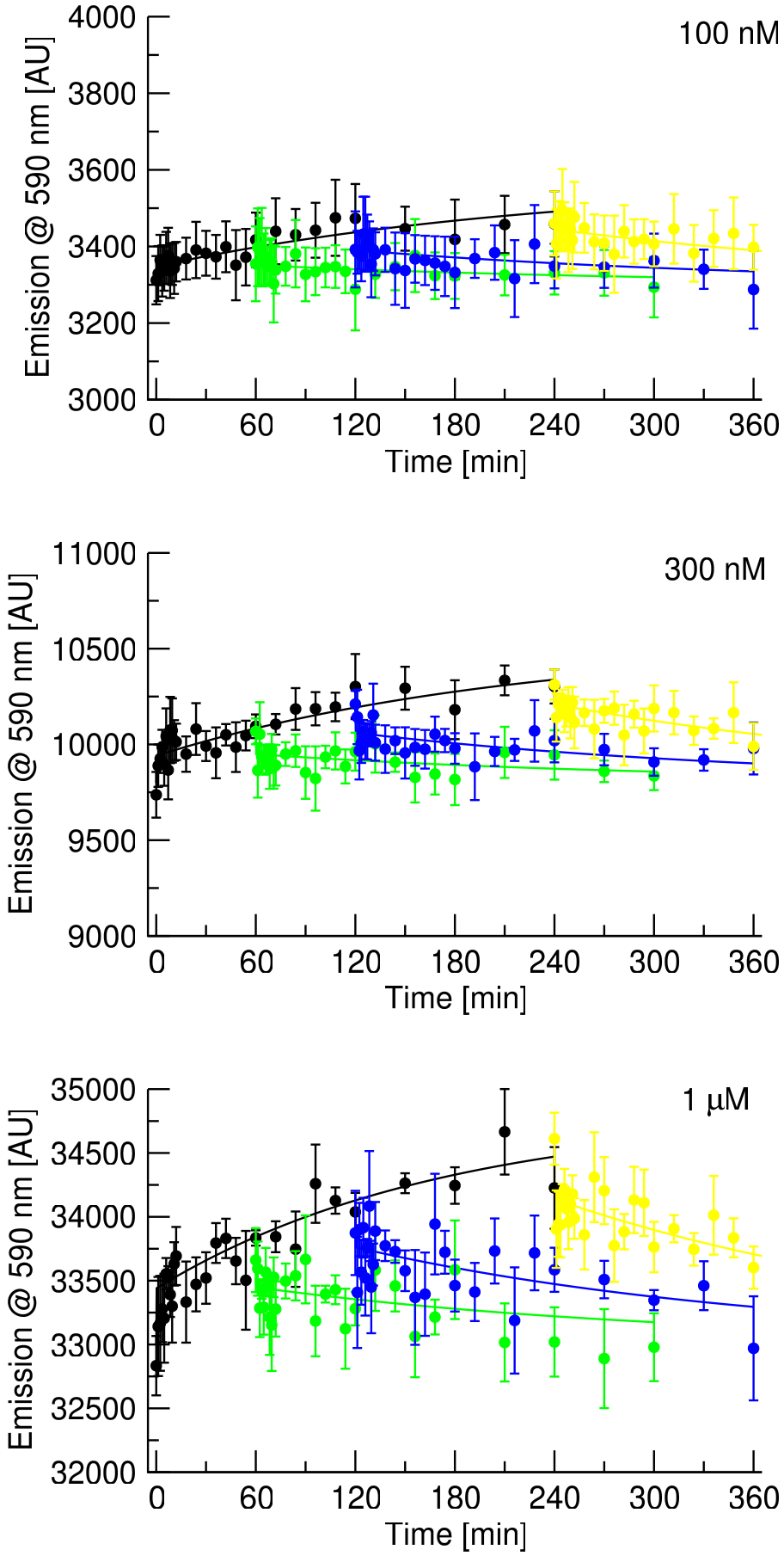
100 nM
Emission @ 590 nm [AU]
4000
3800
3600
3400
3200
3000
0
60
120
180
240
300
360
Time [min]
300 nM
Emission @ 590 nm [AU]
11000
10500
10000
9500
9000
0
60
120
180
240
300
360
Time [min]
1 µM
Emission @ 590 nm [AU]
35000
34500
34000
33500
33000
32500
32000
0
60
120
180
240
300
360
Time [min]

Fig. 9

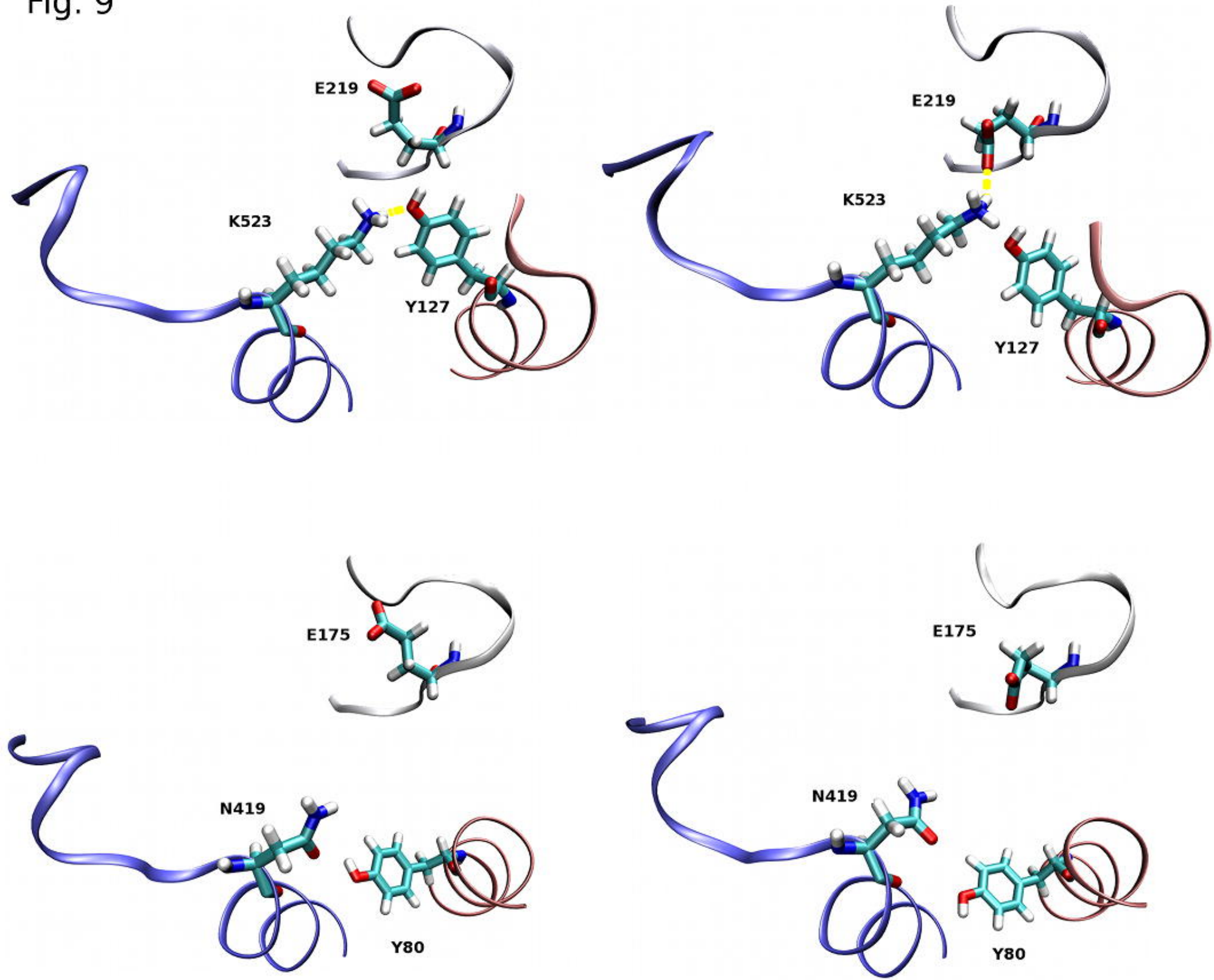

Fig. 10

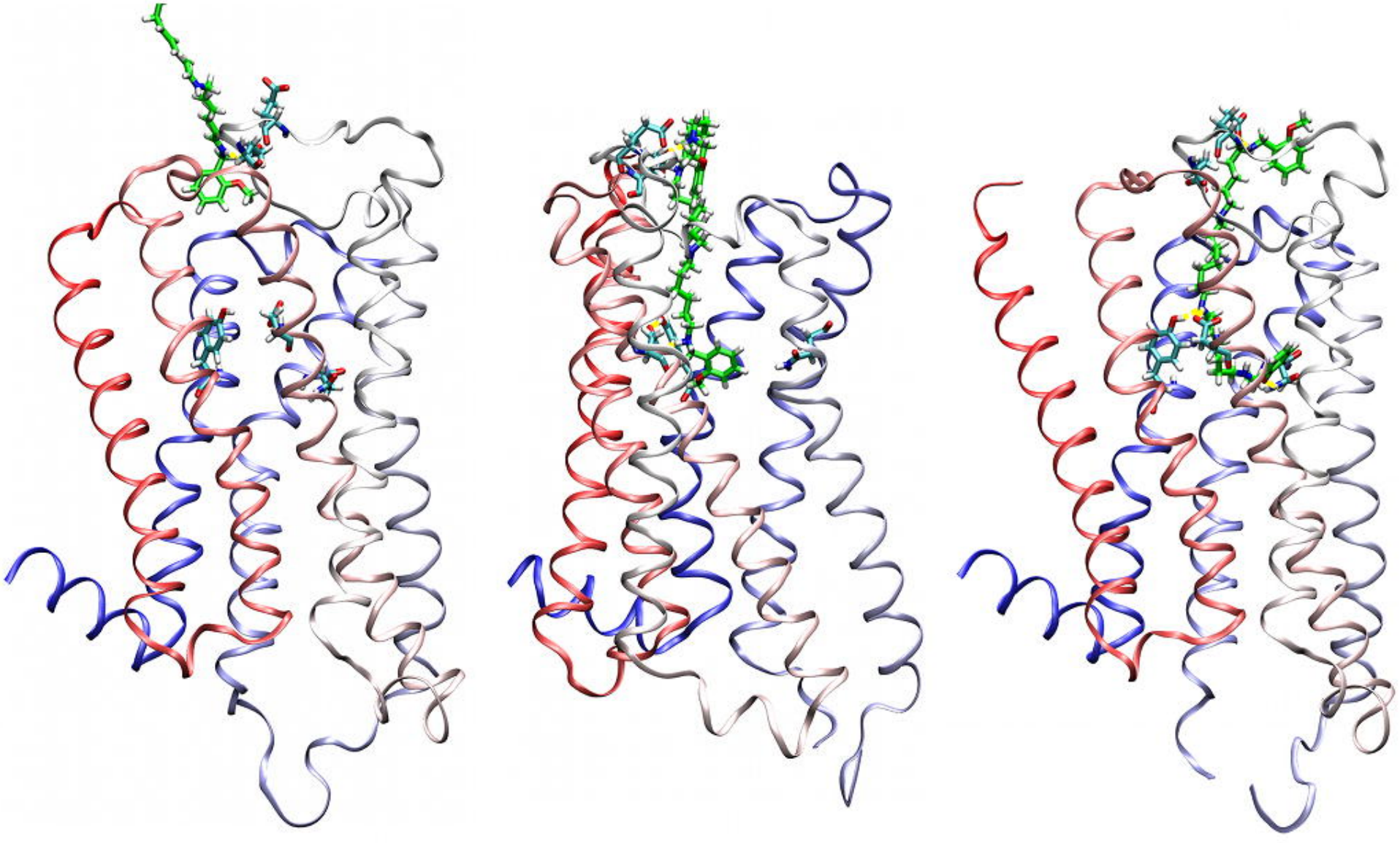

Fig. 11

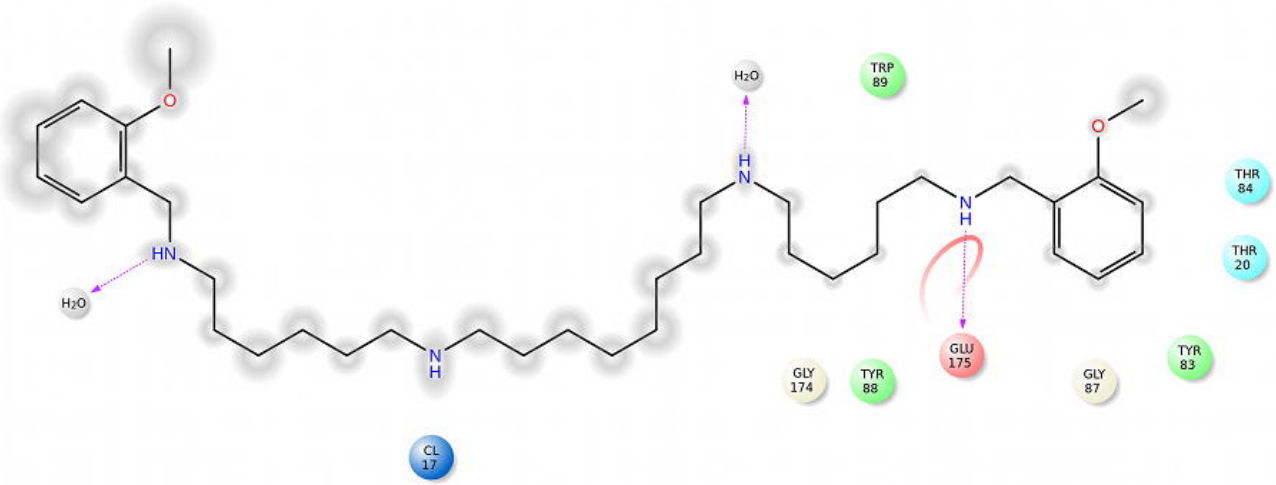
O
HN
H2O
N
H
H2O
TRP 89
H
N
N
H
O
THR 84
THR 20
GLU 175
TYR 83
GLY 174
TYR 88
GLY 87
CL 17

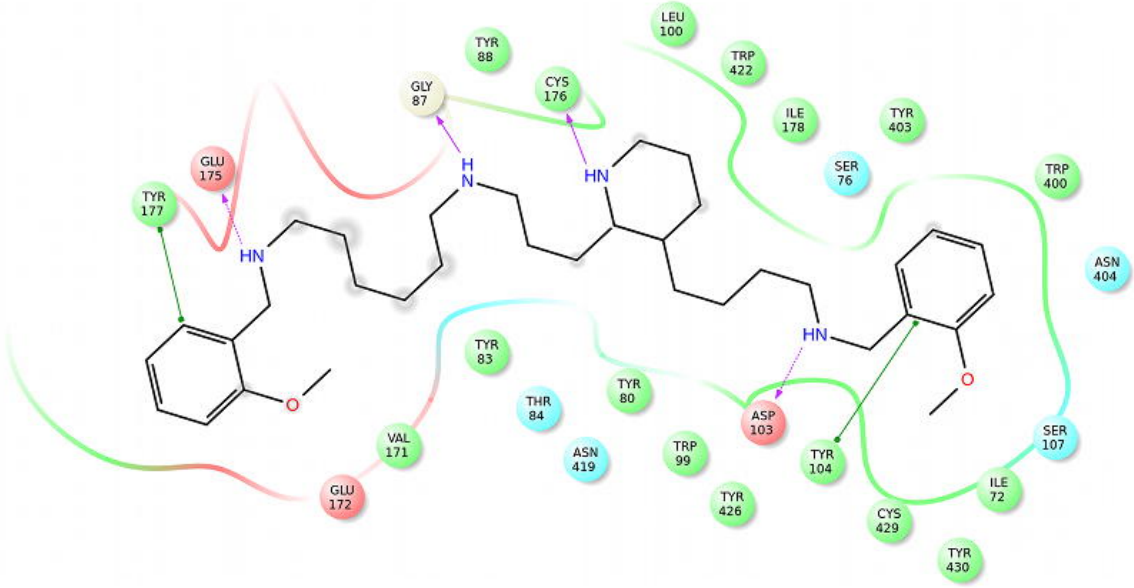
LEU 100
TYR 88
TRP 422
GLY 87
CYS 176
ILE 178
TYR 403
GLU 175
H
N
HN
SER 76
TRP 400
TYR 177
HN
ASN 404
HN
TYR 83
TYR 80
THR 84
O
ASP 103
VAL 171
ASN 419
TRP 99
TYR 104
SER 107
GLU 172
TYR 426
ILE 72
CYS 429
TYR 430

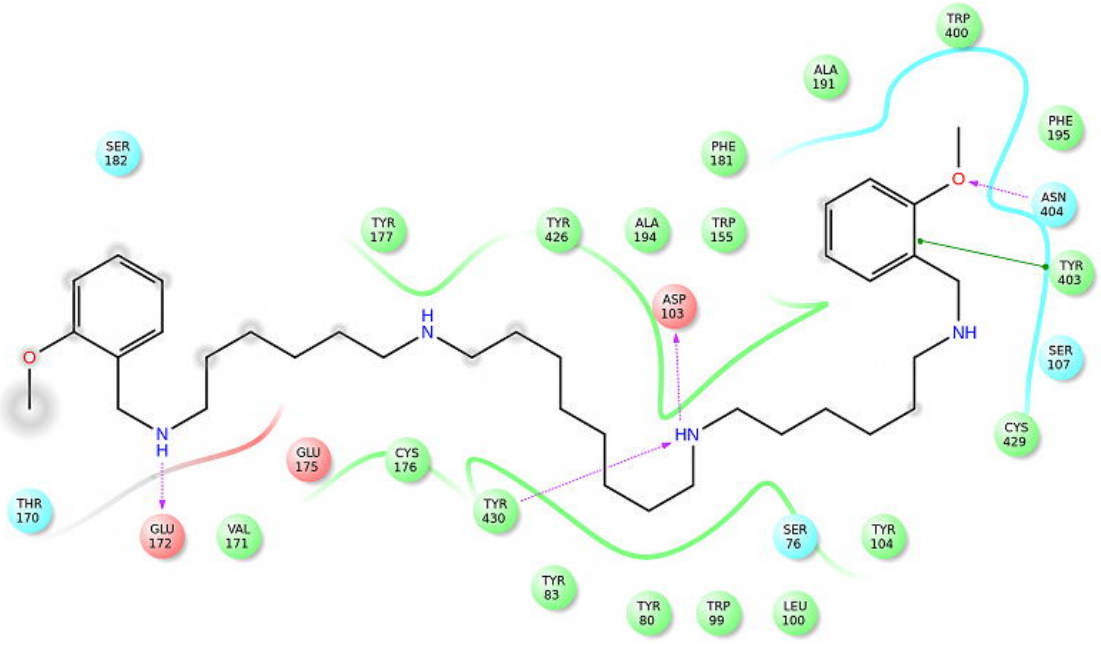
TRP 400
ALA 191
PHE 195
SER 182
PHE 181
O
ASN 404
TYR 177
TYR 426
ALA 194
TRP 155
TYR 403
H
N
ASP 103
NH
SER 107
O
N
H
HN
CYS 429
GLU 175
CYS 176
THR 170
TYR 430
GLU 172
VAL 171
SER 76
TYR 104
TYR 83
TYR 80
TRP 99
LEU 100